Assessment of Regional Land Cover Fractions of Mongolian Semiarid and Arid Area Based on Multi-channel Radiance Data

January 2007

Byambakhuu ISHGALDAN

Assessment of Regional Land Cover Fractions of Mongolian Semiarid and Arid Area Based on Multi-channel Radiance Data

A Dissertation Submitted to

the Graduate School of Life and Environmental Sciences,

the University of Tsukuba

In Partial Fulfillment of the Requirements

for the Degree of Master in Science

(Doctoral program in Geoenvironmental Sciences)

Byambakhuu ISHGALDAN

Abstract

Semiarid and arid ecosystems present high spatial complexity of land use on the globe. Remote measurements of dominant land cover fractions (LCFs) such as photosynthetic vegetation (PV), nonphotosynthestic vegetation (NPV) and bare soil communities are critical for understanding regional climate regime of spatial and regional scales and land-use controls over the functional properties of arid and semiarid ecosystems of Mongolia.

In Mongolia, previous efforts focused on land degradation assessment, vegetation cover monitoring, drought assessment, and desertification monitoring in ecosystem have used the NDVI images derived from AVHRR/NOAA, Landsat TM image and ground truth data with meteorological data calculated by traditional multispectral classification approaches, spectral mixture model, and greenness equations. Indeed, previous efforts considered for detection of only the 'green' part of the vegetation using metric such as normalized difference vegetation index (NDVI), thus yields limited information on the presence and condition of plants in these ecosystems. Nevertheless, monitoring of PV, NPV and bare soil are needed to understand a range of ecosystem characteristics. Under such situations, estimation methodology and technique for dominant land cover fractions are required to improve that including volume of 'dead' part of vegetation and bare soil part. Because estimation of these parts are most important factor to provide the details of biogeophysical information, which effective for an approaching important changes in vegetation properties that can occur in the spatial and regional scales of land-use and biogeochemical cycling.

Therefore, main objective of this study is to determine the regional LCFs of semiarid and arid area of Mongolia using multi-channel radiance data, by adopting methods of general probabilistic spectral mixture model (SUM) and bi-directional distribution function. Additionally, we applied supervised classification method (SCM)

with maximum likelihood analysis to digital camera images for estimating land cover fractions.

An arid and semiarid area of Mongolia was chosen for investigation in the present study. A field vegetation properties and spectral dataset of PV, NPV, and bare soils were complied for 50 semiarid and arid ecosystems of Mongolia, representing wide type of data structure of plant species, vegetation conditions, and soil properties

The results of this present study indicate follow as: (i) the bidirectional distribution function model can work in shortwave-infrared spectral region, because comparison of predicted spectral reflectance value and measured spectral reflectance value are quit agreed each other ; (ii) a conservative value of 50 runs number is enough in Monte Carlo analysis for using SUM to determine land cover fractions value, because in Monte Carlo analysis, most important factor to consider is the minimum number of runs, in the SUM needed to converge to give mean and standard deviation. This analysis is indicated that additional runs beyond 40 have little effect on derived land cover fractions; (iii) the accuracy of the supervised classification method is highly dependent on the section of specific area on image and the individual user. Also the supervised classification method has the disadvantages of too much time and energy and the applications of this method are limited: (iv) the correlation coefficient of land cover fractions calculations using visually determined and the different methods for determining the LCFs can be summarized as SUM (R=0.98) > SCM (R=0.88) for PV, SUM (R=0.5) > SCM (R=0.4) for NPV and SUM (R=0.93) > SCM (R=0.80) for bare soil. Root mean square error of supervised classification method is less than the spectral unmixing model in arid area and more than spectral unmixing model in semiarid area. These results confirm that the spectral unmixing model including Monte Carlo analysis has the higher accuracy for estimation of land cover fractions better than supervised classification method in the study areas. However, application of the spectral unmixing model needs further improvement and more

data and some additional spectral measurements. This is very fundamental research effort in Mongolian pastureland ecosystem.

Keywords: *Land covers fractions, spectral unmixing approach, semiarid, and arid area*

List of Contents

Abstract……..... i
List of Contents……. iv
List of tables…….. vi
List of figures……. vii
List of abbreviations……..... x

1 Introduction……..... 1
1-1. General background……..... 1
1-2. Background of previous study……. 2
1-3. Purpose of the study……..... 5

2 Methods…….. 6
2-1. Description of the study area…….. 6
2-1-2.Climate description of the study area…….. 9
2-1-3. Vegetation condition of the study area……. 11
2-2. Field observation……..... 16
2-2-1. Spectral reflectance……. 16
2-3. Data processing……. . . ……. 20
2-3-1. Bi-directional reflectance model……. 20
2-3-2. Spectral unmixing model……..... 22
2-3-2-1. Monte Carlo analysis……... 25
2-5-4. Supervised classification method…… 27

3. Results and Discussions……. 31
3-1. Soil properties……. 31
3-2. Soil textural classes……..... 32
3-3 Analysis of spectral shape……... 40
3-4. Effect of noise on cover fractions……... 47
3-5. Bi-directional reflectance correction…….. 51

3-6. Derived Land covers fractions from spectral unmixing approach……. 53
3-7 Derived Land covers fractions from supervised classification method…….. 61
3-8 Relationship between visually determined land cover fractions and different model results……..... 67

Conclusions…… 69

Acknowledgements……. 71

References…….. 72

List of Tables

Table 1 The name and abbreviation of field sites…….. 8
Table 2 The dominant vegetation species in study area……... 15
Table 3 Description of field sites investigated to collect LCFs, biomass, and soil moisture…….. 19
Table 4 Soil chemical property analysis……. 33
Table 5 Effects of noise on calculated cover fractions using tied and derivative spectra……. 49
Table 6 Correlation matrixes of derived land cover fractions from different viewing angle…….. 58
Table 7 Summary statistics of derived land cover fractions from different viewing angle in semiarid area……. 59
Table 8 Summary statistics of derived land cover fractions from different viewing angle in arid area……. 60
Table 9 Correlation coefficients of estimating LCFs from different methods……... 68
Table 10 RMSE of estimating LCFs from different methods…… 68

List of Figures

Figure 1 The elevation map of Mongolia with river network based on GIS data set (Saandar and Sugita, 2004) of Mongolia. The study areas were divided into semiarid and arid area. The main study areas are shows with stars and circle symbol on this map. The study area name listed in abbreviation of site name Table 1. …… 7

Figure 2 The annual precipitation map of Mongolia with river network based on GIS data set (Saandar and Sugita, 2004) of Mongolia. The study areas were divided into semiarid and arid area. The main study areas are shows with stars and circle symbol on this map……. …….. …….. 10

Figure 3 The vegetation zone map of Mongolia with river network based on GIS data set (Saandar and Sugita, 2004) of Mongolia. Study area were located very various vegetation transect zone belonging to semiarid and arid area of Mongolia. The main study areas are shows with stars and circle symbol on this map…… 12

Figure 4 Top side, panel (a) shows the vegetation distribution in semiarid area based on GIS data set (Saandar and Sugita, 2004) of Mongolia. Observation area is shown by blue circles. Panel (b) shows digital camera image of KBU 11 site… 13

Figure 5 Top side, panel (a) and (c) are show the vegetation distribution in arid area based on GIS data set (Saandar and Sugita, 2004) of Mongolia. Observation area is shown by blue circles. Panel (b) and (d) are show digital camera image of MNG 2 and BGN 4 sites.. …….……. 14

Figure 6 Illustrations of bidirectional reflectance measurement. Panel (a) shows pattern of bidirectional reflectance measurement with different viewing angles at 8 different sun azimuths. Panel (b) shows measured points of bidirectional reflectance measurement and inside of circle viewing angle from 30, 50 and 70 degrees from surface. Panel (c) shows measurement bidirectional reflectance action with photo. ……..……..…….. 18

Figure 7 A schematic of the spectral unmixing algorithm and its processing steps. 24

Figure 8 Illustrations of Monte Carlo analysis and its proceeding steps. (Probability density functions of f(x), which described by spectral reflectance of endmember) ……..……..……... 26

Figure 9 Illustrations of the random selection…… 27

Figure 10 Intensity, Hue, and Saturation Color Coordinate System…….. 30

Figure 11 The soil triangle. Each triangle is shows soil texture of observed area within semiarid area. From top side up bottom, panels are indicating KBU site, JRN site, UND site DRN site and BRN site. ……..……... 36

Figure 12 The dynamics of soil moisture and dry biomass of photosynthetic vegetation. The soil moisture is measured from same soil textural like, sandy loam soil and different soil class from semiarid area. Site name listed in abbreviation of site name table. ……..……..…… 39

Figure 13 Typical reflectance of photosynthetic vegetation collected at semiarid and arid area of Mongolia. Full range of variability is shown. …… 41

Figure 14 Typical reflectance of bare soil collected at semiarid and arid area of Mongolia. Full range of variability is shown……..…… 41

Figure 15 Typical reflectance of photosynthetic vegetation in SWIR spectral region is shown. ……..……..……. 42

Figure 16 Typical reflectance of bare soil in SWIR spectral region is shown. …… 42

Figure 17 Typical reflectance of PV (dotted), NPV (solid), and bare soil (dashed) in SWIR region …….……..…….. 44

Figure 18 The tied reflectance of photosynthetic vegetation collected at semiarid and arid area of Mongolia. SWIR range of variability is shown. ……. 45

Figure 19 The derivative reflectance of photosynthetic vegetation collected at semiarid and arid area of Mongolia. SWIR range of variability is shown. …….. 45

Figure 20 The tied reflectance of bare soil collected at semiarid and arid area of Mongolia. SWIR range of variability is shown. ……..…….. 46

Figure 21 The derivative reflectance of bare soil collected at semiarid and arid area of Mongolia. SWIR range of variability is shown. ……..…….. 46

Figure 22 Mean and standard deviation of each endmember fractions number of runs in MCU procedure. ……..……..…… 50

Figure 23 Bi-Directional Reflectance Distribution curve and comparison between predicted and observed reflectance values on the SWIR spectral region. Semiarid (a), and Arid (b). ……..……..…… 52

Figure 24 Comparison of predicted photosynthetic vegetation values, calculated by AutoMCU method and visually determined photosynthetic vegetation values. The both of semiarid and arid area are shown……..……. 55

Figure 25 Comparison of predicted nonphotosynthetic vegetation values, calculated by AutoMCU method and visually determined nonphotosynthetic vegetation values. The both of semiarid and arid area are shown…….. 56

Figure 26 Comparison of predicted bare soil values, calculated by AutoMCU method and visually determined bare soil values. The both of semiarid and arid area are shown ……..……..…….. 57

Figure 27 Typical land cover fractions at KBU site 1 in semiarid area. From top side panel (a) is show digital camera image of KBU 1; panel (b) is show image is transformed IHS color image from RGB color image; and panel (c) is classified image using supervised classification method. …….……. 62

Figure 28 Typical land cover fractions at MNG site 1 in arid area. From top side panel (a) is show digital camera image of KBU 1; panel (b) is show image is transformed IHS color image from RGB color image; and panel (c) is classified image using supervised classification method. …….. 63

Figure 29 Comparison of predicted photosynthetic vegetation values, calculated by supervised classification method and visually determined photosynthetic vegetation values. The both of semiarid and arid area are shown…….. 64

Figure 30 Comparison of predicted nonphotosynthetic vegetation values, calculated by supervised classification method and visually determined nonphotosynthetic vegetation values. The both of semiarid and arid area are shown 65

Figure 31 Comparison of predicted bare soil values, calculated by supervised classification method and visually determined bare soil values. The both of semiarid and arid area are shown……..…….. 66

List of Abbreviations

BRN	Baga Nuur
BRDF	bidirectional reflectance distribution function
DRN	Darkhan
DNG	Dund Gobi
IHS	insensity, hue and saturation
JRN	Jargaltkhaan
KBU	kherlen Bayan-Ulaan
LCFs	land cover fractions
MNG	Mandali Gobi
NPV	nonphotosynthestic vegetation
NIR	near infrared region
NDVI	normalized difference vegetation index
PV	photosynthetic vegetation
RAISE	The Range land Atmosphere-Hydroshpere-Bioshpere Interaction Study Experiment in Northeastern Asia
RGB	red, green and blue
SWIR	shortwave infrared region
SCM	supervised classification method
SUM	spectral unmixing model
SMA	spectral mixture analysis
UND	Undurkhaan

Introduction

1-1. General background

Recently, land degradation process, particularly, land cover fractions (LCFs) changes in ecosystem due to anthropogenic, global warming impact, drought and pasture land grazing have received much more attention of scientists from different countries of the word. These factors possible affects land degradation process by exchanging the atmosphere-hydrosphere-biosphere cycle and surface energy balance of both regional and spatial scales in arid and semiarid region. Because dominant land cover communities has been playing an important role in the transfer of matter and energy from the Earth's surface to the atmosphere. Moreover, interactions between the land surface and the atmosphere, and the resulting exchanges of energy and water have a large effect on typical LCFs.

Mongolia is a landlocked country, which has dry and continental climate because of high altitude and big distance from seas, ocean and surrounded by high mountains. Mongolia has expansive areas (almost 90%) of natural grasslands and current dominant industry in the agricultural sector of the country is the nomadic livestock husbandry which is highly dependent upon the conditions and changes in nature and the environment during the four seasons of a year. Almost 99% of the arid and semi-arid areas in Mongolia consist of natural pasture (Shiirevdamba, 1998). On the other hand, Mongolian traditional animal husbandry is heavily dependent on pasture which depends on weather conditions of a year. Therefore, land degradation problems have been receiving more consideration focus of recently scientists' studies. The grazing factor should be the driver factor of all factors causing land degradation. Indeed, grazing has increased during long time by nomadic herd activities. Therefore, grazing process is main anthropogenic factor that affects LCFs in ecosystem. In fact, LCFs are more difficult to determine and measure accurately among many parameters of dominant land cover fractions communities at the field site. However,

these fractions communities are can be divided into three main categories such as photosynthetic vegetation (PV), nonphotosynthetic vegetation (NPV), and bare soil.

In this context, this study focused on determination of regional LCFs of semiarid area of Kherlen river basin and arid area of Gobi region of Mongolia using multi-channel radiance data, by adopting methods of general probabilistic spectral mixture model developed by Asner and Lobell (2000), bi-directional distribution function (Rahman et al, 1993), and also we applied supervised classification method with maximum likelihood analysis to digital camera image for estimating LCFs.

1-2. Background of previous study

In Mongolia, several studies involving the use of the NOAA/AVHRR data have been published. Most of them had concerned with determining vegetation cover and pasture land changes and its monitoring study (Oyun *et al.,* 1994; Adyasuren and Bayarjargal, 1995; Bayarjargal, 1995, M. Erdenetuya, 2004). Recently, Adyasuren and Bayarjargal (1995) mapped drought conditions of the Central Asian zone based on the multi-temporal Global Vegetation Index data from 1982-1987 and noticed that when a drought events occur in Mongolian Gobi Desert zone, the Normalized Difference Vegetation Index (NDVI) values became to a low values, 0.0-0.05 units, same as value of the extra-arid land - Taklimakan Desert. Erdentuya (2004), and Adyasuren et al, (2005) have presented determination of land cover types using pasture land map based on higher resolution Landsat TM image and lower resolution NOAA/NDVI data integrated with ground measurements of pasture biomass data.

Arid and semiarid ecosystems present high spatial complexity of land use in the globe. Typically LCFs such as photosynthetic vegetation (PV), nonphotosynthestic vegetation (NPV) and bare soil of vary at scale smaller than size of the typical remote sensed pixel, making it difficult to measure these key indicators of ecosystem structure

directly and accurately with conventional remote sensing approach. Many applications have been devised to analyses PV, NPV and bare soil cover fractions in semiarid and arid regions. A wide variety of studies have attempted to correlate vegetation indices (e.g., NDVI) to the fractional coverage of PV and bare soil (Carlson and Ripley, 1997). The general spectral regions used to detect PV and visible and near-infrared wavelengths (400-1300 nm) in fact, which do not easily separate the individual contribution of NPV and bare soil to the measurement (Asner 1998, Asner et al 2000). More recently, spectral mixture analysis (SMA) was developed to decompose image pixels into PV, NPV and bare soil covers. There are many SMA efforts applied in semiarid and arid regions using airborne and space borne sensors. SMA is a technique for deriving subpixel LCFs by converting spectral reflectance value to cover fractions of specified land surface, called "endmembers". One of the main successfully techniques uses endmember "spectral bundles" and that account for the natural variability of endmembers occurring in natural (Bateson et al, 2000). Because there are a number of endmember combinations that can produce any spectral signal, a wide range of acceptable unmixing results for any reflectance pixel are possible (Asner and others 2000). However, to address SMA uncertainty, Asner and Lobell (2000) and Asner and Heidebrecht (2002) provided a detailed description of general probabilistic linear spectral mixture model based on Monte Carlo analysis, which accounts for natural variability of endmembers thought the calculation of uncertainty for each pixel endmember constituent.

There are several studies investigated field measurement of vegetation fractional coverage using a digital camera has been recognized as a new method in recent years. The soil and vegetation can be easily distinguished using an image from a digital camera. White et al (2000) measured the vegetation fractional coverage in the shrubbery grassland in semiarid ecosystem of New Mexico, USA. Their research proved that the use of digital camera to determine the vegetation fractional coverage of the surface of semiarid

ecosystem is reliable and effective (White et al 2000). Zhou et al (1998) had used various methods of field measurement, including ocular estimation, the sampling belt, and photographic methods to estimate the vegetation fractional coverage of semiarid ecosystem in Australia. Their investigation proved that different surface measuring methods may lead to significantly different measurement outcomes, and that this different would be exacerbated when study area being measured is large. At present, the most common method used to calculate the vegetation fractional coverage using digital camera images includes ocular estimation and supervised classification (White et al 2000).

As mentioned, previous works to estimate changes of land degradation assessment, vegetation cover monitoring, drought assessment, and desertification monitoring in ecosystem usually using the NDVI images derived from AVHRR/NOAA, Landsat TM image and ground true data including meteorological data calculated by traditional multispectral classification approaches, spectral mixture model, and greenness equation in Mongolia. Since above applications are, that possible for analyzing spatial vegetation pattern and for assessing for changes of ecosystem dynamics. However, previous efforts have not provided the detailed biogeophysical information needed to monitor and model important changes in vegetation properties that can occur in the spatial and regional scales of land use and biogeochemical cycling. Indeed, detection of only the 'green' part of the vegetation using metric such as normalized difference vegetation index (NDVI) thus yields limited information on the presence and condition of plants in these ecosystems. Monitoring of both PV and NPV is needed to understand a range of ecosystem characteristics including vegetation presence, coverage and abundance, physiological and biogeochemical functioning, drought severity and pasture land grazing, etc. On this situation, estimation methodology and technique for dominant LCFs are required to improve the typical LCFs. An estimation methodology and technique should be assessed

the impact of comprehensive extent in space and time of main factors in the arid and semiarid area of Mongolia.

1-3. Purpose of the study

The main objective of this study was to calculate regional LCFs using various methods and to discussed advantages and drawbacks of these methods to develop more suitable model for estimating LCFs and to determine changes extent and density of LCFs at different ecosystems in Mongolia. This research can be achieved by following specific purposes.

- To apply/test bi-directional reflectance function to make correction for field spectral measurements data for the spectral unmixing model.

- To employ/test probabilistic spectral unmixing model for determining the LCFs of semiarid and arid ecosystems of Mongolia.

- To use supervised classification method for determining the LCFs of semiarid and arid ecosystems of Mongolia using a digital camera image.

2 Methods

2-1. Description of study area

An arid and semiarid area of Mongolia was chosen for investigation in the present research. Abbreviation of the study area is listed in Table 1. The semiarid area is located in Kherlen river basin in northeastern part of Mongolia and its surrounding regions have been selected as the study area, which are located in the Khentii province of Mongolia. These area's altitude ranges were from 1470 m at MNG site though 1035 m at UND site. The longitude was between 108.36 and 110.62 E degree and then latitude was from 46.63 to 47.78 N degrees.

The arid area is located in an arid area of the Dund-Gobi province of Mongolia. An elevation ranges were about from 1302 to 1504 m and the longitude was between 106.23 and 106.47 E degree and latitude was from 45.94 to 45.67 N degrees.

Additionally, also we investigated in Bulgan, in South Gobi, which is located in an arid area of Mongolia. This area longitude was between 103.57 and 103.70 E degree and then latitude was from 44.25 to 44.01 N degrees and elevation range was about from 1123 to 1423m. Figure 1 shows the elevation map of Mongolia with river networks.

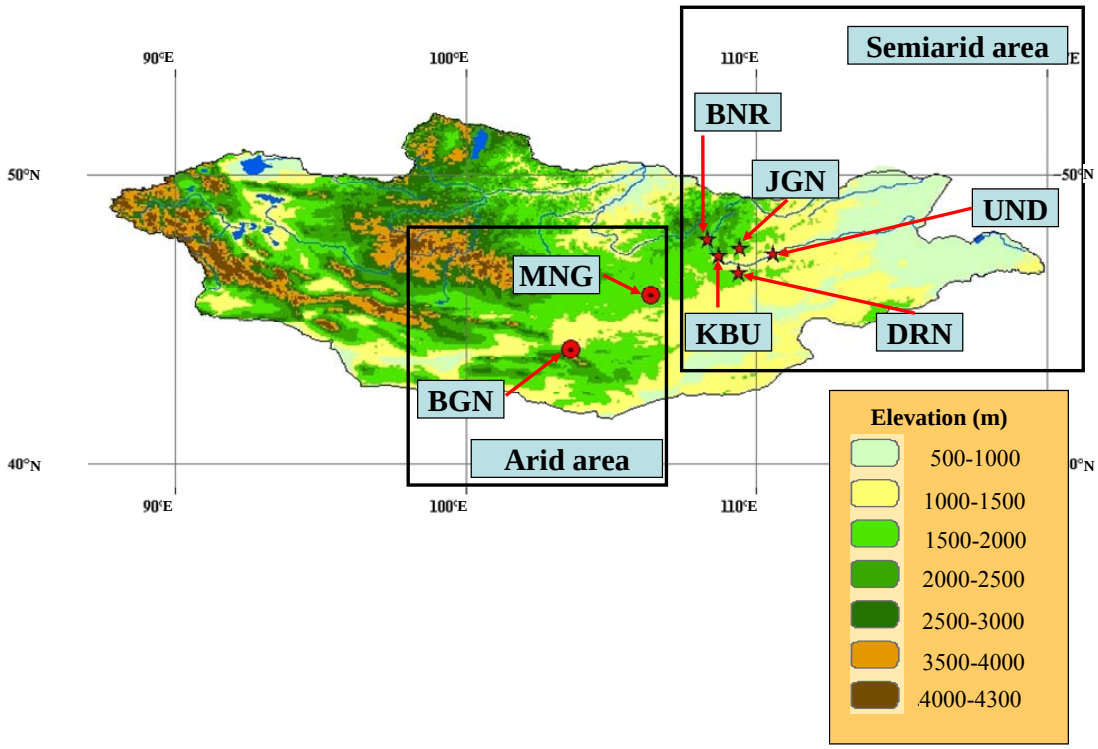

Figure 1 The elevation map of Mongolia with river network based on GIS data set (Saandar and Sugita, 2004) of Mongolia. The study areas were divided into semiarid and arid area. The main study areas are shows with stars and circle symbol on this map. The study area name listed in abbreviation of site name Table 1.

Table 1 The name and abbreviation of field sites

Study area name	Abbreviation	Location		Altitude (m)
		Longitude	Latitude	
Kherlenbayan-Ulaan	KBU			1251
Jargaltkhaan	JGN	108.73	47.21	1325
Undurkhaan	UND	110.62	47.30	1031
Darkhan	DRN	109.41	46.63	1250
Baganuur	BNR	108.36	47.78	1350
Mandaligobi	MNG	106.40	45.86	1467
Bulgan	BGN	103.65	44.01	1450

2-1-2. Climate description of study area

Study areas were located in northeastern part and south part of Mongolia. The main characteristics of the climate of Mongolia are sunny days, long and cold winters. The average mean air temperature in the warmest month is 15-20°C in the semiarid area, and 20-25°C in the arid area of Mongolia. In the arid and semiarid areas, the summer continues over 3 months. The maximum summer air temperature can reach anywhere 35-39°C in the semiarid and 38-41°C in the arid area. As can be seen in Figure 2, annual precipitation map (Saandar and Sugita, 2004), the total annual precipitation in mountainous regions averages to about 400 mm, in the steppe 150-250 mm and in the desert-steppe less than 100 mm. About 85 to 90 per cent of the precipitation falls during the three summer months (Shiirevdamba, 1998). The number of rainy days decreases from north to south. The temporal and spatial distribution of precipitation in Mongolia is variable. There is very little precipitation at the beginning of the growing season but much more in the second half of the season when cool air starts to spread around the country. This variation has considerable effects on the growth of several spring plants. Summer, autumn and winter precipitation is a source of soil moisture but it is insufficient for vegetation to thrive in this country.

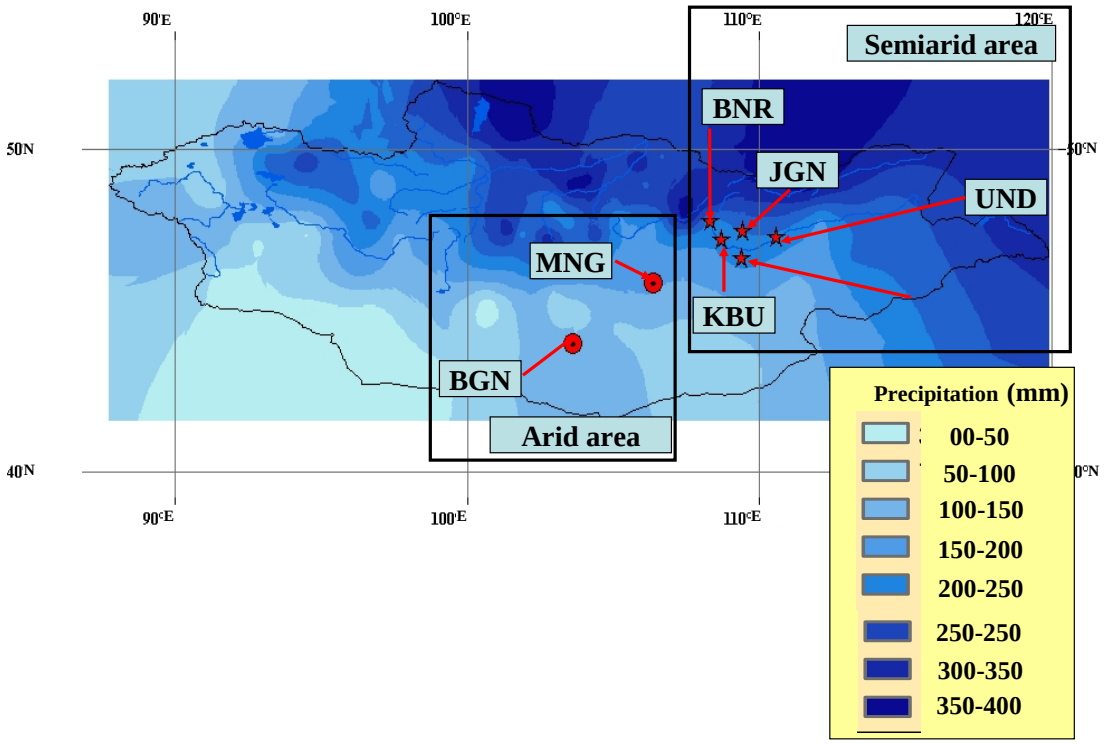

Figure 2 The annual precipitation map of Mongolia with river network based on GIS data set (Saandar and Sugita, 2004) of Mongolia. The study areas were divided into semiarid and arid area. The main study areas are shows with stars and circle symbol on this map.

2-1-3. Vegetation condition of the study area

Arid and semiarid ecosystems endure strong temporal and spatial variation of climate and very pressure effects of land use that affects unique dynamic typical land cover, leaf area characteristics. Biophycical properties of typical land cover such as PV, NPV and bare soil was compiled for 50 arid and semiarid area of Mongolia, representing a wide array of plant growth forms and species, vegetation condition, and soil mineralogical-hydrological properties.

As mentioned above, there are very different vegetation species and land coverage within and between study areas (Figure 4-5). One of our study areas was established by RAISE project (The Range land Atmosphere-Hydroshpere-Bioshpere Interaction Study Experiment in Northeastern Asia) and it would be advantage to collect the data of atmosphere and hydrosphere cycle of the northeastern part of Mongolia, where AWS (automatic weather station) was founded by RAISE project. These areas were located at vegetation transition zones under semiarid climate.

The semiarid area is a specific region by ecosystems and the climate characteristics (Adyasuren et al, 2005), which located in Kherlen river basin in northeastern part of Mongolia. Generally, vegetation types can be classified into 3 categories (figure 3), such as forest mountain steppe, meadow steppe, steppe and dry steppe in this area. However, vegetation species are depending on vegetation transition zones within this area.

In arid area, vegetation types are classified into 3 categories, which are short-type grass, long-type glass, which vegetation species are depends on vegetation transition zones within this area.

Additionally, we have to collect more dominant and widely distributed vegetation species from field sites, collected by Chen et al (2003) from semiarid area and Ouyansubd and Byambakhuu (2006) from arid area. The dominant vegetation species are listed in Table 2.

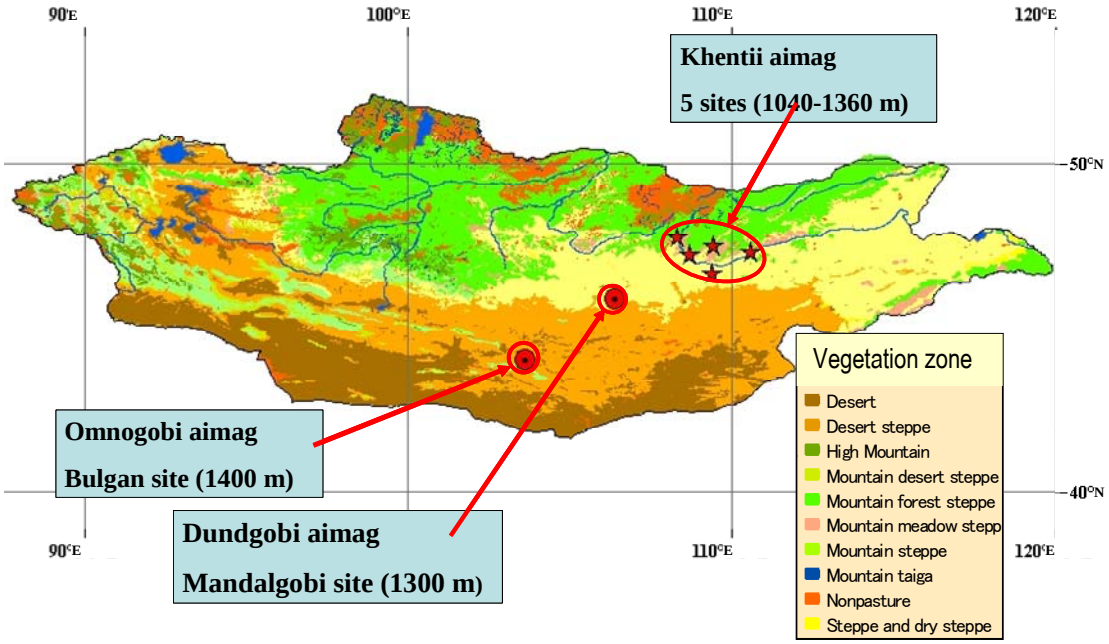

Figure 3 The vegetation zone map of Mongolia with river network based on GIS data set (Saandar and Sugita, 2004) of Mongolia. Study area were located very various vegetation transect zone belonging to semiarid and arid area of Mongolia. The main study areas are shows with stars and circle symbol on this map.

a)

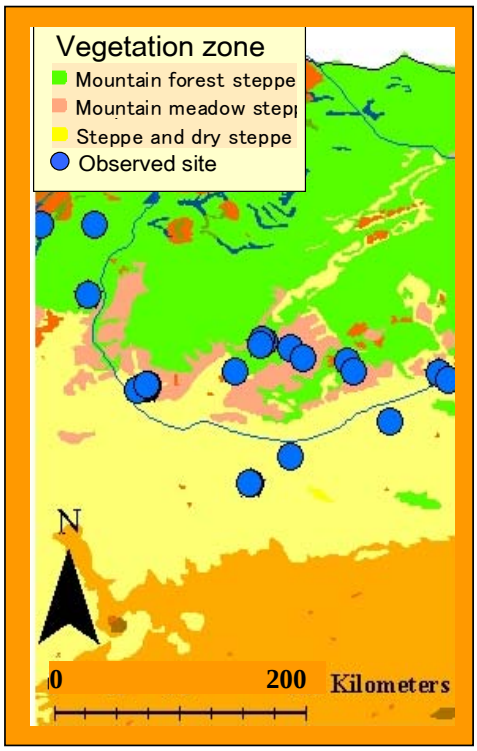

b)

Figure 4 Top side, panel (a) shows the vegetation distribution in semiarid area based on GIS data set (Saandar and Sugita, 2004) of Mongolia. Observation area is shown by blue circles. Panel (b) shows digital camera image of KBU 11 site.

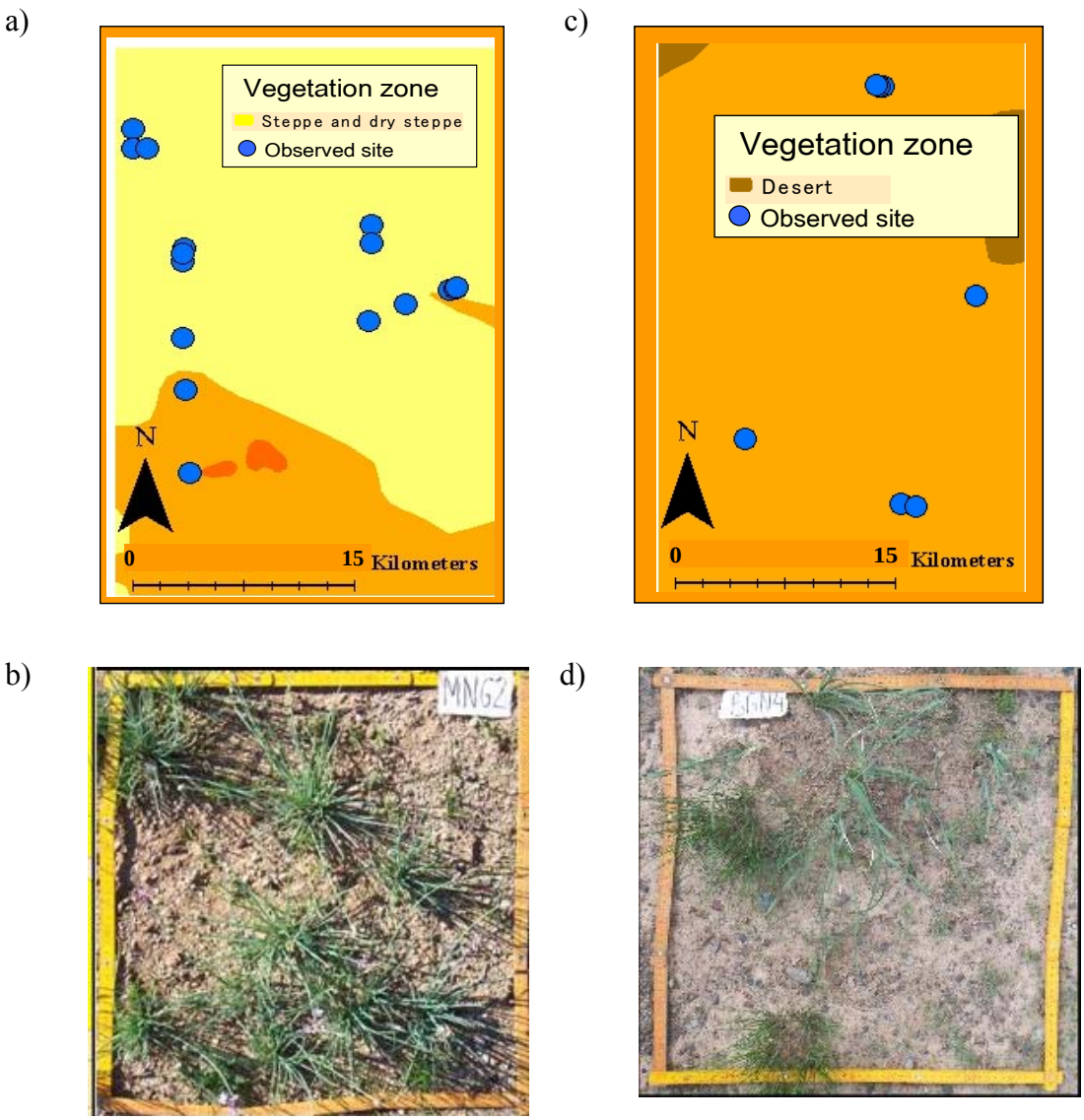

Figure 5 Top side, panel (a) and (c) are show the vegetation distribution in arid area based on GIS data set (Saandar and Sugita, 2004) of Mongolia. Observation area is shown by blue circles. Panel (b) and (d) are show digital camera image of MNG 2 and BGN 4 sites.

Table 2 The dominant vegetation species in study area.

Dominant vegetation species	
Semiarid area	**Arid area**
Caragana microphylla	*Allium Polyrhizum*
Stipa Krylovii Roshev	*Allium Mongolicum*
Carex Duriuscula	*Stipa Gobica*
Caragana pygmaea	*Artemisia*
Ders	*Peganum Negillastrum*
Kochai	*Iris Bungei*
Leymus chinenensis	*Carex Stenophylloides*
Stellaria dichotoma	*Haplophyllum Dahuricum*
Potentilla anserina	*Sasola Collina*
	Caragana microphylla
	Caragana leucophloea

2-2. Field observation

2-2-1. Spectral reflectance

The semiarid and arid area of Mongolia was chosen for investigation in the present study and the 'Fieldspec' was used in ground-based observations. In our study, we tried to find different biophysical properties of an experimental area within study area such as strong differences in PV cover between sites and pronounced differences in NPV between sites. The size of area was 50x50 cm.

We have to collect more dominant and widely distributed vegetation species from field sites, collected by Chen et al (2003) from semiarid area and Ouyansubd and Byambakhuu (2006) from arid area, which are listed in Table 2. Also we have to measured soil moisture and biomass of PV and NPV, and LCFs was determined by visually (Table 3). We used TDR instrument for measuring soil moisture of observed area. Mainly, we carried out bi-directional reflectance spectrometry over study sites. The spectral data were collected for a full range from 350nm to 2500 nm by a spectrometer with 8 ^{o} sensor fore optic attached. The resolution of wavelength is 10 nm. 8 azimuth view angles (solar direction and every 45^0 from solar direction) were selected. Then a sensor viewing angle was hold at 30^0,50^0 and 70^0 in each diagonal for 8 azimuth angles (figure 6). The observations were performed during daytime between 9 and 19-hour local time. A series of observation took around 20 minutes, which depend on solar condition. 24 effective series of data were obtained in the intensive observation in 2005 from semiarid area and 26 series of data in 2006 from arid area of Mongolia. Radiance measurements were converted to reflectance using a white panel, which were measured immediately before each canopy or soil measurement. We measured to separately that reflectance of PV and NPV endmember using additional device of "fieldspec" spectrometer.

At the time of the field survey, both of semiarid and arid areas were fully green, allowing us to separate the spectra both by PV and NPV group. In additional, spectral reflectance properties of bare soil patches were measured at each sampling locations along each transect. Also we tried to take accurate value of LCFs communities in all selected area using digital camera at each sampling site in study area by use of a global positioning system (GPS) in Figure 1-5. The area of each quadrate was 50x50 cm and the LCFs communities of these areas were taken using a digital camera. The digital camera was held 1 m above the selected area and then images were taken nadir-looking at the each area. The resulting images were stored.

a)

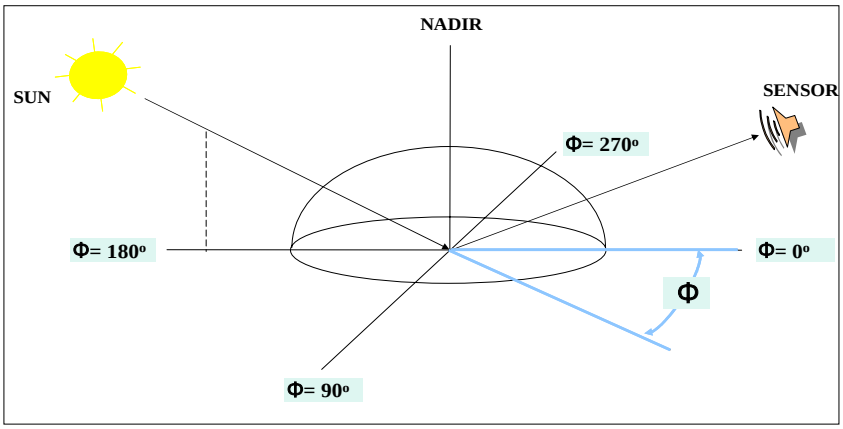

b)

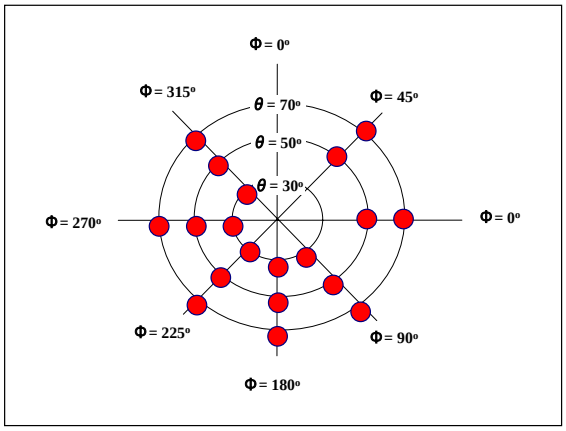

c)

Figure 6 Illustrations of bidirectional reflectance measurement. Panel (a) shows pattern of bidirectional reflectance measurement with different viewing angles at 8 different sun azimuths. Panel (b) shows measured points of bidirectional reflectance measurement and inside of circle viewing angle from 30, 50 and 70 degrees from surface. Panel (c) shows measurement bidirectional reflectance action with photo.

Table 3. Description of field sites investigated to collect LCFs, biomass, and soil moisture.

Site name	Data of measurement	Location		Altitude (m)	Sky condition	Biomass (g/0.25)		LCFs			Soil moisture
		Lon	Lat			PV	NPV	PV	NPV	BS	
KBU1	7/31/2005	108.74	47.22		Cloudy	16.9	33.5	35	55	10	9
KBU 2	7/31/2005	108.74	47.21		Cloudy	18.4	52.8	45	50	5	10
KBU 3	7/31/2005	108.75	47.23		Cloudy	15.2	24.1	38	42	20	8
KBU 4	7/31/2005	108.74	47.22		Cloudy	12.2	20.6	30	15	55	12
KBU 5	7/31/2005	108.74	47.22		Cloudy	7.7	13.4	32	18	55	9
KBU 6	7/31/2005	108.74	47.22		Clear	13.9	27.3	25	15	60	10
KBU 7	1/8/2005	108.73	47.21		Clear	7.9	54.9	35	50	15	10
KBU 8	1/8/2005	108.73	47.21		Cloudy	7.3	3.5	40	10	50	9
KBU 9	1/8/2005	108.71	47.21	1237	Cloudy	36.8	4.7	70	5	25	8
KBU10	1/8/2005	108.71	47.21	1238	Cloudy	14.3	7.3	75	5	20	8
KBU11	1/8/2005	108.67	47.21	1216	Cloudy	34	129.2	57	40	3	9
JGN1	2/8/2005	109.31	47.31	1260	Clear	9.1	24.2	45	25	30	14
JGN2	2/8/2005	109.47	47.49		Clear	12.8	2.5	60	5	35	13
JGN3	2/8/2005	109.50	47.50	1320	Clear	11.2	0.9	60	5	35	36
JGN4	2/8/2005	109.48	47.51	1327	Cloudy	10.9	10.7	55	10	35	13
JGN5	2/8/2005	109.47	47.48	1337	Cloudy	26.8	41.6	65	15	20	12
JGN6	2/8/2005	109.47	47.48	1336	Cloudy	17.2	1.4	37	3	60	13
JGN7	3/8/2005	109.47	47.48	1340	Cloudy	27.8	8.9	55	5	40	15
JGN8	3/8/2005	109.66	47.46	1359	Cloudy	42.5	31.6	70	20	10	9
JGN9	3/8/2005	109.74	47.40	1302	Cloudy	42.2	22.3	80	10	10	10
UND1	3/8/2005	110.02	47.38	1039	clear	24.6	11.2	65	10	25	10
UND2	3/8/2005	110.62	47.31	1040	Clear	24.6	2.7	63	2	35	8
UND3	3/8/2005	110.62	47.31	1039	Clear	80.6	76.6	85	5	5	8
UND4	3/8/2005	110.07	47.31	1031	Clear	35.3	57.8	75	10	15	6
UND5	4/8/2005	110.67	47.26	1031	Clear	38	17.2	80	10	10	8
UND6	4/8/2005	110.30	47.01	1078	Clear	17.2	15.2	60	5	35	9
DRN1	4/8/2005	109.66	46.80	1136	Clear	21.7	4	65	5	30	6
DRN2	4/8/2005	109.66	46.80	1135	clear	4.8	3.8	20	3	77	6
DRN3	4/8/2005	109.41	46.63	1261	Clear	8.2	2.2				6
DRN4	4/8/2005	109.40	46.64	1251	Clear	18.7	4.3	60	10	30	6
DRN5	4/8/2005	109.40	46.64	1250	Cloudy	8.4	2.8	75	5	20	8
BNR1	6/8/2005	108.06	48.21	1357	Cloudy	44.9	16.8	80	10	10	7
BNR2	6/8/2005	108.40	48.21	1359	Cloudy	16.9	6.3	65	5	30	6
BNR3	6/8/2005	108.36	47.78	1361	Cloudy	51.1	2.2	80	5	15	7
MNG1	2/8/2006	106.36	45.88		Clear	11.56	0.8	41	5	54	7
MNG2	2/8/2006	106.41	45.85		Clear	12.4	0.76	80	1	19	6
MNG3	2/8/2006	106.27	45.73		clear	9.13	0.68	45	1	54	8
MNG4	2/8/2006	106.27	45.84		Clear	15.65	1.13	52	3	35	7
MNG5	2/8/2006	106.27	45.83		Clear	16.48	1.58	80	5	15	6
MNG6	2/8/2006	106.27	45.84		Clear	20.99	1.18	55	3	47	5
MNG7	2/8/2006	106.28	45.66		Clear	35.02	0.02	96	1	4	8
MNG8	2/8/2006	106.41	45.79		clear	20.56	3.38	30	5	65	7
MNG9	3/8/2006	106.24	45.94		Clear	45.67	20.09	90	5	5	7
MNG10	3/8/2006	106.24	45.92		Clear	10.50	2.31	85	5	10	6
MNG11	3/8/2006	106.25	45.92		Clear	13.12	1.06	70	5	25	7
MNG12	3/8/2006	106.27	45.77		Clear	6.65	0.7	40	5	55	6
MNG13	3/8/2006	106.47	45.81		clear	12.71	0.15	40	5	55	6
MNG14	3/8/2006	106.47	45.81		Clear	8.55	0.03	30	5	65	9
MNG15	3/8/2006	106.47	45.81		Clear	11.16	0.03	25	5	70	6
MNG16	3/8/2006	106.43	45.80		Clear	32.43	1.33	90	5	5	7
MNG17	3/8/2006	106.43	45.80		Clear	16.46	1.12	35	5	60	8
BGN1	5/8/2006	103.66	44.01		clear	9.85	0.12	35	5	60	6
BGN2	5/8/2006	103.66	44.01		Cloudy	12.52	0.29	80	5	15	7
BGN3	5/8/2006	103.57	44.05		Cloudy	3.83	0.75	50	5	45	9
BGN4	5/8/2006	103.70	44.13		Cloudy	8.32	1.63	90	5	55	8
BGN5	5/8/2006	103.64	44.25		Cloudy	4.1	4.65	20	5	75	4
BGN6	5/8/2006	103.64	44.25		Cloudy	4.85	0.56	10	5	85	6
BGN7	5/8/2006	103.64	44.25		Cloudy	5.63	8.1	15	5	80	6

2-3. Data processing

In this study, we attempted the determination of regional LCFs of semiarid and arid area of Mongolia using multi-channel radiance data, by adopting methods of general probabilistic spectral mixture model developed by Asner and Lobell (2000), bi-directional distribution function (Rahman et al, 1993). Additionally, we applied supervised classification method with maximum likelihood analysis to digital camera image for estimating LCFs.

2-3-1. Bi-directional reflectance model

Almost all of material covering earth surface have characteristic of reflectance which depend on the viewing angle of sensor and the solar zenith angle, and uniform characteristics of reflectance, called Lambertian surface, is merely found. This kind of angular characteristic is called by bidirectional reflectance. Previous efforts have experimentally showed bidirectional reflectance distributions of surface reflectance (Kimes et al., 1983). There are several models of bidirectional reflectance distribution function (BRDF) developed for uniform surface (Roujean, et al., 1992, Rahman, et al., 1993, Susaki, et al., 2004). We prepared spectral dataset using bi-directional distribution function model (BRDF). We used a model, developed by Rahman et al (1993), because this model was more suitable to correction for bidirectional reflectance. BRDF is shown by following equations.

$$\rho\left(\theta_s \ddot{e} \theta_v \ddot{e} \phi\right) = \rho_o \frac{\cos\theta_s^{\kappa-1}\cos\theta_v^{\kappa-1}}{\left(\cos\theta_s + \cos\theta_v\right)^{1-\kappa}} F\left(g\right)\left[1 + R\left(G\right)\right] \quad (1)$$

$$F\left(g\right) = \frac{1 - \Theta^2}{\left[1 + \Theta^2 - 2\Theta\cos\left(\pi - g\right)\right]^{1.5}} \quad (2)$$

$$R = \frac{1 - \rho_0}{1 + \left[\tan^2\theta_s + \tan^2\theta_v - 2\tan\theta_s \tan\theta_v \cos\phi\right]^{\frac{1}{2}}} \quad (3)$$

$$g = \cos\theta_s \cos\theta_v + \sin\theta_s \sin\theta_v \cos\phi \quad (4)$$

where ρ is reflectance at solar zenith angle θ_s and viewing zenith θ_v, and ϕ is the viewing azimuth from solar direction clockwise, and R expresses the hot spot effect, which is extremely high reflectance at round counter side of the sun. Three unknown parameters Θ, ρ_0, k have to be determine according to observed conditions. In this study, these three parameters were determined with the field spectral data obtained over steppe, desert steppe and bare soils. All parameter are parameterized by the solar zenith angle.

Thus, using this model, we can get vegetation information and to generate standard condition for corrected dataset from field spectral database.

2-3-2. Specral unmixing model

Most spectral mixture models represent the reflectance of image pixel as a linear combination of endmember spectra and this main equation can be written as

.

$$\rho_{(pixel)} = \sum_{e=1}^{n} \left[C_e \cdot \rho(\lambda) \right] = \left[C_{pv} \cdot \rho_{pv}(\lambda) + C_{npv} \cdot \rho_{npv}(\lambda) + C_s \cdot \rho_s(\lambda) \right] + \varepsilon(\lambda)$$

$$\sum_{e=1}^{n} [C_e] = 1 \qquad (5)$$

where ρ and C are the reflectance of and cover fractions of each endmember, and ε is error term of the solution at wavelength (λ).

Given an input corrected spectra reflectance derived from bi-directional reflectance measurements of field spectral measurement ($\rho_{(\lambda)\mathrm{pixel}}$) and three endmember reflectance bundles ($\rho_{\mathrm{veg}}(\lambda)$, $\rho_{\mathrm{soil}}(\lambda)$ and $\rho_{\mathrm{NPV}}(\lambda)$), the model is used to estimate for LCFs (C_{veg}, C_{soil} and C_{NPV}). On the other hand, Spectral unmixing model output was calculated subpixel LCFs values with statistic confidence intervals. Because the goal of this research was to develop suitable method for estimate LCFs and to determine extent and density of land cover changes at different ecosystems.

A schematic diagram of the SUM algorithm and its processing steps are shown in Figure 7. This algorithm is used to correct spectral reflectance data of a pixel, calculated by BRDF, inducing PV, NPV, and bare soils information (top right), and derived endmember's reflectance bundles of PV, NPV, and bare soils are inputs to the model (top left). Indeed, endmember spectra set is randomly selected from each endmember bundle, and the pixel deconvolution is calculated iteratively using Monte Carlo technique.). Finally, we needed to test, that spectral unmixing model is how much sensitive and difference for final results using widely distributed 2 kinds of vegetation species derived

from study area. Therefore, we generated the endmember bundles of the PV and NPV, it derived from *Stipa Krylovii* Roshev species, because it was widely distributed vegetation within semiarid area. Moreover, *Allium Mongolicum* vegetation was selected for generating endmember bundles of the PV and NPV in the arid area. In case of bare soil, each of observed sites data was selected.

Using both of these two kinds of the reflectance data, we applied to spectral unmixing model and land cover fractions were determined.

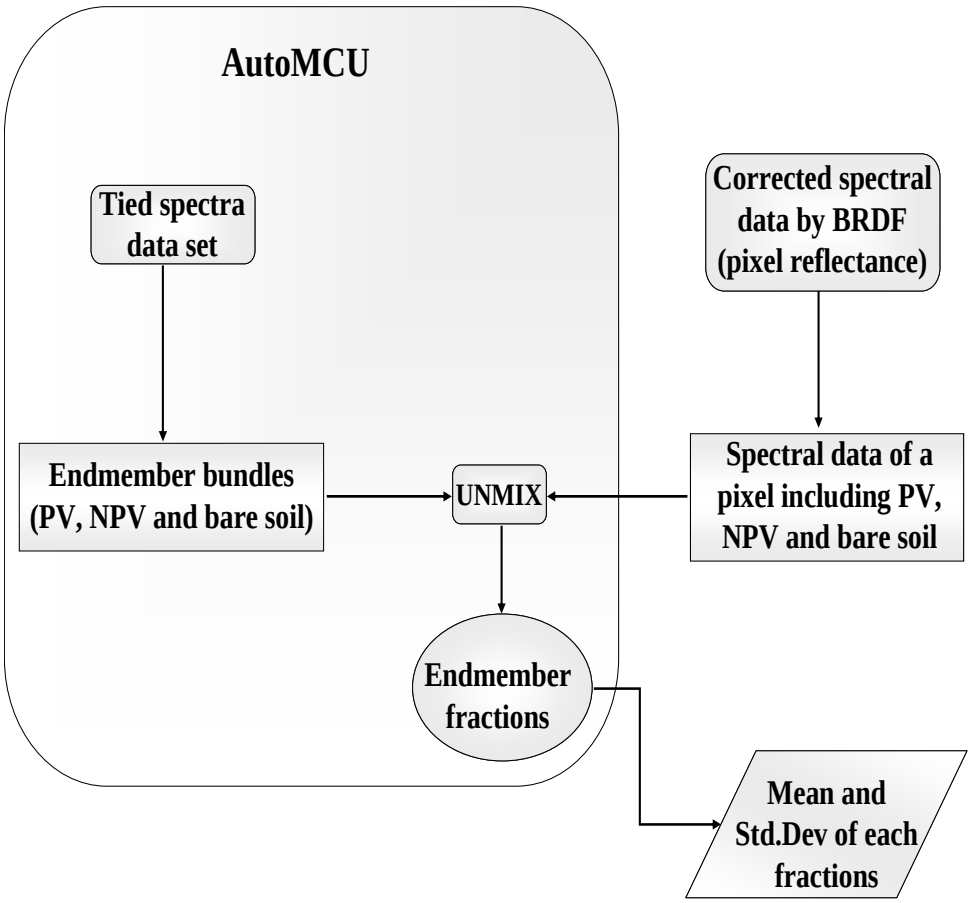

Figure 7 A schematic diagrams of the spectral unmixing algorithm and its processing steps.

2-3-2-1. Monte Carlo analysis

Figure 8 shows the general idea of the Monte Carlo simulation as applied to arbitrary physical system. Assuming that the evolution of physical system can be described by probability density functions (pdf's), the Monte Carlo simulation can proceed by sampling from these pdf's, which necessitates fast and effective way to generate random numbers uniformly distributed in the interval [0,1]. Then outcomes of these random samplings, must be accumulated in an appropriate manner to produce the desired results, but essential characteristic of the Monte Carlo is the used of random sampling techniques to arrive at solution of the physical problem. Because purpose of the Monte Carlo method is to determine true value of physical system, but true value is unknown.

In our study, we tried to derive subpixel cover fractions with statistical confidences interval using Monte Carlo technique. Using this technique, we can generate large number of endmember combinations for each pixel by randomly selecting spectra from the 200 dataset of field spectra.

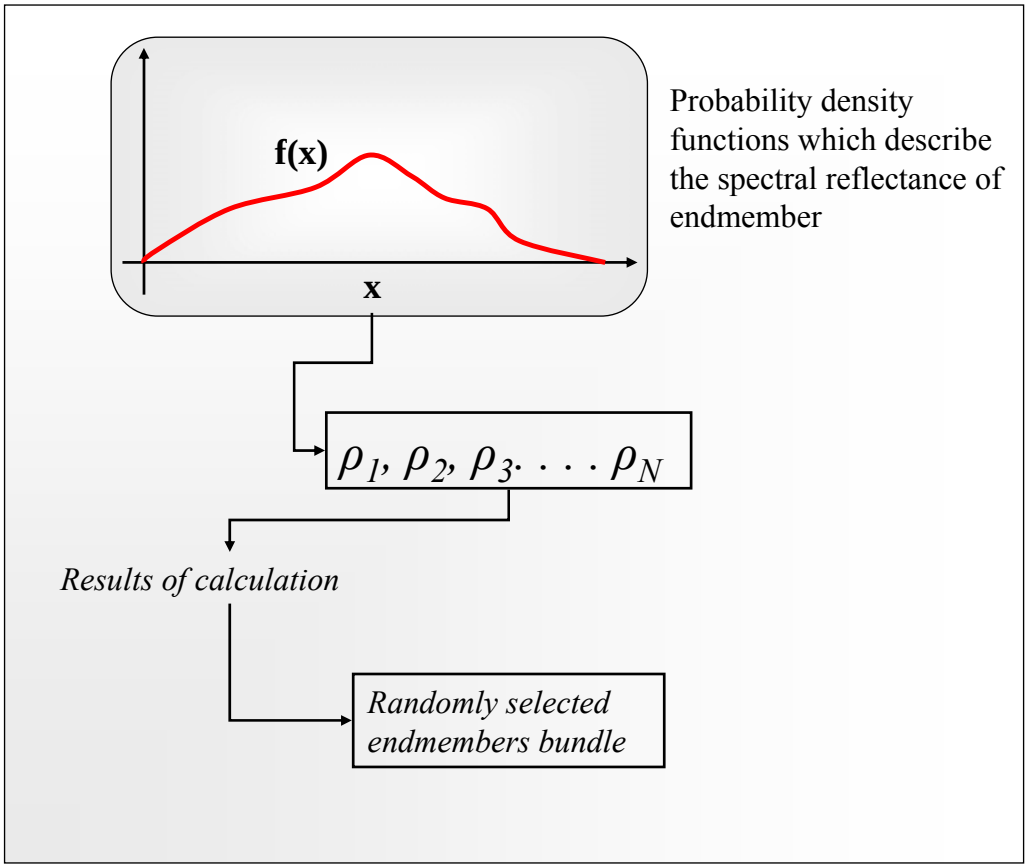

Figure 8 Illustrations of the Monte Carlo analysis and its proceeding steps. (Probability density functions of f(x), which described by spectral reflectance of endmember)

2-3-4. Supervised classification method

Calculation of LCFs using SCM with digital camera images has been used in many studies (Li, 2002). With the support of ERDAS IMAGINE 9.0 image processing software, the representative LCFs training sampling areas are selected on digital color image. There are many ways to express the color space of given color, most of which are applicable to different situations (Healey 1989). However, the image processing systems have three color guns. These correspond to red, green, and blue (RGB), the additive primary colors. However, to reduce of each characteristic component in space the RGB color system, it is usually necessary to change RGB to other color characteristic color space. However, it is possible to define an alternate color space that uses intensity (I), hue (H), and saturation (S) as the three positioned parameters (in lieu of R,G, and B). Because, this system is advantageous in that it presents colors more nearly as perceived by the human eye. Defination of (I), hue (H), and saturation (S) (IHS) can be written as:

- Intensity is the overall brightness of the scene (like PC-1) and varies from 0 (black) to 1 (white).
- Saturation represents the purity of color and also varies linearly from 0 to 1.
- Hue is representative of the color or dominant wavelength of the pixel. It varies from 0 at the red midpoint through green and blue back to the red midpoint at 360. It is a circular dimension (Figure 9).

In Figure 8, 0 to 255 is the selected range; it could be defined as any data range. However, hue must vary from 0 to 360 to define the entire sphere. Mainly, the IHS color space system is very suitable for the image processing procedure based on human visual features of color reorganization. Therefore, we have to changed RGB image to IHS image using ERDAS IMAGINE 9.0 image processing software. First, digital color image

were converted into RGB space and then to IHS space. Secondly, SCM was applied with the maximum likelihood method to the IHS images and then results can be obtained classified land cover fractions values.

The algorithm used in the Image Interpreter RGB to IHS transform is given as:

$$R = \frac{M - r}{M - m} \qquad G = \frac{M - g}{M - m} \qquad B = \frac{M - b}{M - m} \tag{6}$$

Where: R,G,B are each in the range of 0 to 1.0, r, g, b are each in the range of 0 to 1.0, M = largest value, r, g, or b, m = least value, r, g, or b. At least one of the R, G, or B values is 0, corresponding to the color with the largest value, and at least one of the R, G, or B values is 1, corresponding to the color with the least value.

The equation for calculating intensity in the range of 0 to 1.0 is:

$$I = \frac{M + m}{2} \tag{7}$$

The equations for calculating saturation in the range of 0 to 1.0 are:

$$S=0, \qquad \text{If } M=m$$

$$S = \frac{M - m}{M + m}, \qquad \text{If } I<0.5 \tag{8}$$

$$S = \frac{M + m}{2 - M - m}, \qquad \text{If } I>0.5$$

The equations for calculating hue in the range of 0 to 360 are:

$$\begin{aligned} &\text{If } M = m,\ H = 0 \\ &\text{If } R = M,\ H = 60\,(2 + b - g) \\ &\text{If } G = M,\ H = 60\,(4 + r - b) \\ &\text{If } B = M,\ H = 60\,(6 + g - r) \end{aligned} \tag{9}$$

where R,G, and B are each in the range of 0 to 1.0, M = largest value, R, G, or B, m = least value, R, G, or B

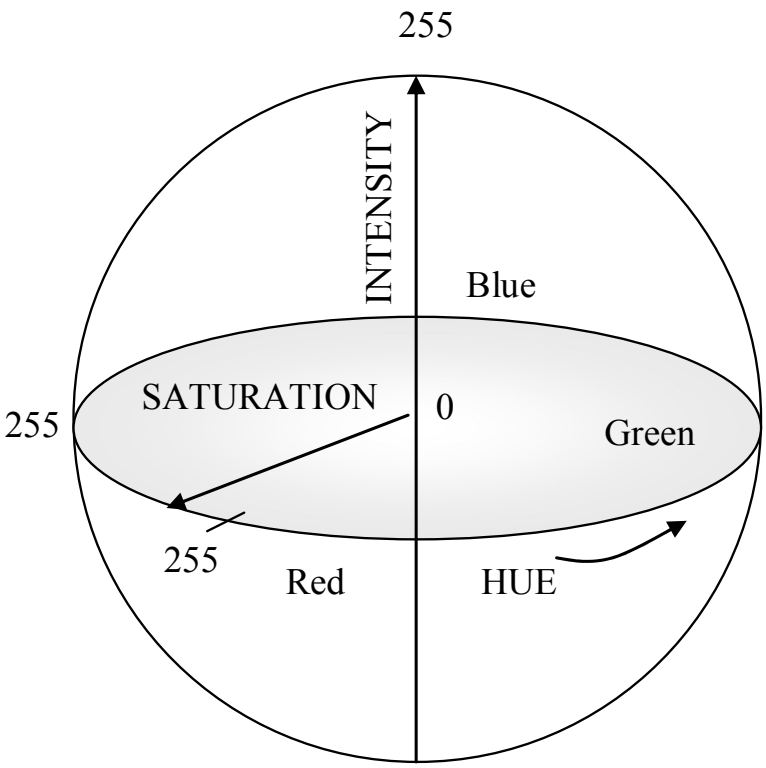

Figure 9 Intensity, Hue, and Saturation Color Coordinate System

3 Results and Discussions

3-1. Soil properties

In this part, we show some results of soil properties data of semiarid area, because the soil properties data are very important factor to understand LCFs general dynamics and it trend in these ecosystems. We had take soil sample were taken from semiarid area in the summer of 2003, by A. Amgalan and I. Byambakhuu. We did not collect soil properties data from arid area yet.

At that time, we took soil samples from the top 40 cm to represent their soil texture, soil structure, soil acidity and plant nutrients. These plant nutrients are humus, total nitrogen, carbonate, phosphorus, potassium, sulfur, calcium and magnesium. The pH was measured with a pH meter and it was between 6.93 and 7.37. Most common microorganisms grow best at pH 6-8. Therefore research area's soil pH is great for microorganisms' growth. Generally value of humus contents of 3-8 percent or higher in the soil improve plant growth, but the research area's soil samples' humus contents are 1.63-2.15%. Nitrogen is most often the limiting nutrient plant growth. Soil samples have low total nitrogen supplies, 0.099-0.13%. Other plant nutrients were absorbed carbonate contents of 0.12-3.4%, absorbed calcium contents of 19.9-28.1 mg-eq/100g, magnesium contents of 2.1-5.3 mg-eq/100g, mobile potassium contents of 1.75-3.05mg/100g and mobile potassium contents 3-12 mg/100g. These results are attached in Table 4.

Additionally, we measured soil moisture contents from each observed sites. In water limited systems such as both semiarid and arid area, soil moisture plays a major role in vegetation patterns and type of land cover, and is consequently of primary importance to the ecosystems of these areas. The Figure 11 shows biomass of PV and soil moisture dynamics and these panels are shown soil moisture contents and biomass of PV

are decreasing from semiarid to arid and its depends on receiving of precipitation and soils types with pedogenic horizons, low in organic matter, and dry more than 6 months of the year in all horizons.

3-2. Soil textural classes

Textural names are given to soils based on the relative proportions of each of the three soil separates – sand, silt, and clay.

The textural triangle is used to determine the soil textural name after the percentage of sand, silt, and clay are determined from a laboratory analysis.

In reading the textural triangle, the lines intersect in the sandy loam. Therefore, all the soil samples from observed sites within semiarid area. Soil triangles are shows in Figure 10 According to the soil orders, in semiarid area soil is belonging to Aridisols (A. Amgalan, 2003).

Table 4 Soil chemical property analysis

№	Soil sample	Humus	Total nitroger	Carbonate	Soil acidity	Absorbed			Mobile	
						Ca	Mg	Z	P_2O_5	K_2O
		%			PH	mg -eq/100g			mg/100g	
1	Kherlenbayan-Ulaan 0-20 cm	3.03	0.19	0.096	7.12	16.8	2.9	19.7	2.4	6
2	20-40cm	1.63	0.099	0.12	7.37	19.9	5.3	25.2	1.9	10
3	40-60cm	1.77	0.108	0.12	7.05	17.5	2.9	20.4	2.05	8
4	Baganuur	1.85	0.112	0.76	7.09	28.1	2.1	30.2	3.05	5
5	Darkhan	1.82	0.111	3.4	6.93	27	4.9	31.9	1.95	5
6	Kherlenbayan-Ulaan	1.57	0.095	0.43	7.27	21.1	3.8	24.9	2.55	10
7	Ondorkhaan	1.86	0.113	2.98	7.2	26.8	5.1	31.9	1.85	12
8	Jalgaltkhaan	2.15	0.13	2.98	6.95	25	3.4	28.4	1.75	3

KBU

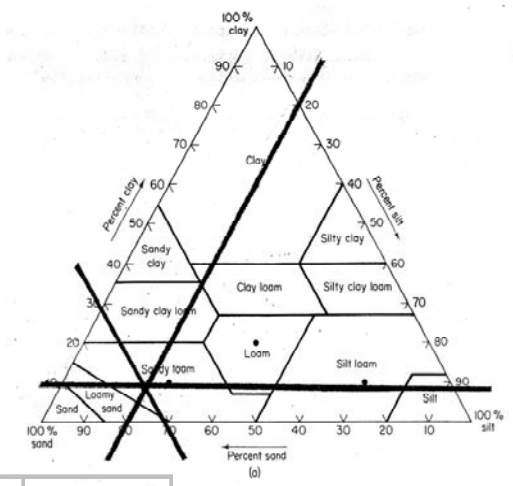

Textural Class	% Sand	% Silt	% Clay
Sandy loam	55	16	29

JGN

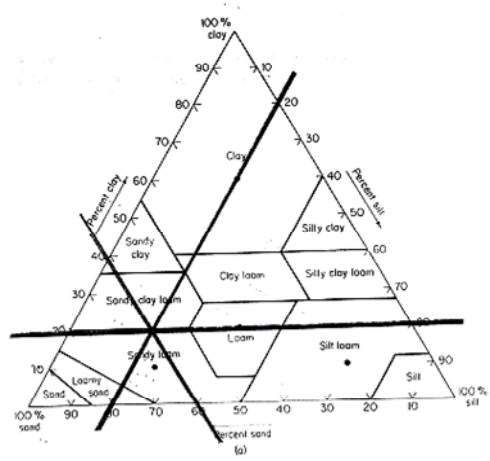

Textural Class	% Sand	% Silt	% Clay
Sandy loam	72	10	18

Figure 10 The soil triangle. Each triangle is shows soil texture of observed area within semiarid area. From top side up bottom, panels are indicating KBU site and JRN site.

UND

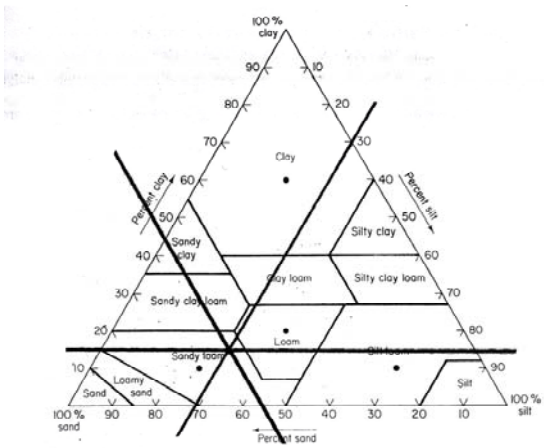

Textural Class	% Sand	% Silt	% Clay
Sandy loam	61	19	20

DRN

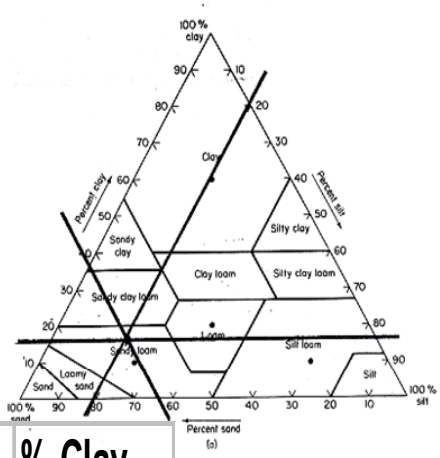

Textural Class	% Sand	% Silt	% Clay
Sandy loam	64	17	19

Figure 10 The soil triangle. Each triangle is shows soil texture of observed area within semiarid area. From top side up bottom, panels are indicating UND site and DRN site.

BRN

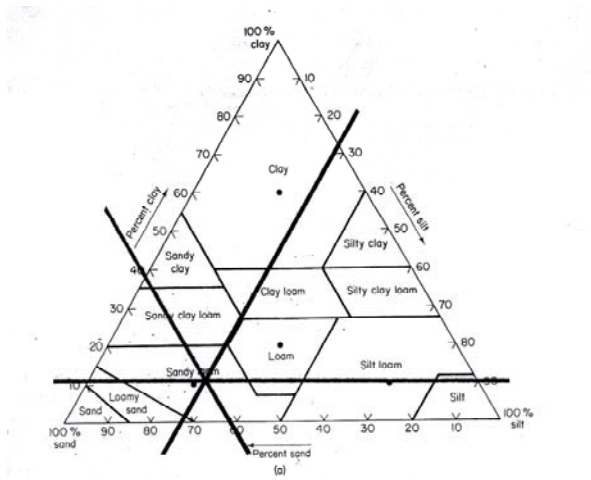

Textural Class	% Sand	% Silt	% Clay
Sandy loam	63	13	24

Figure 10 The soil triangle. Each triangle is shows soil texture of observed area within semiarid area. From top side up bottom, panels are indicating BRN site. Site name listed in abbreviation of site name Table 1.

a)

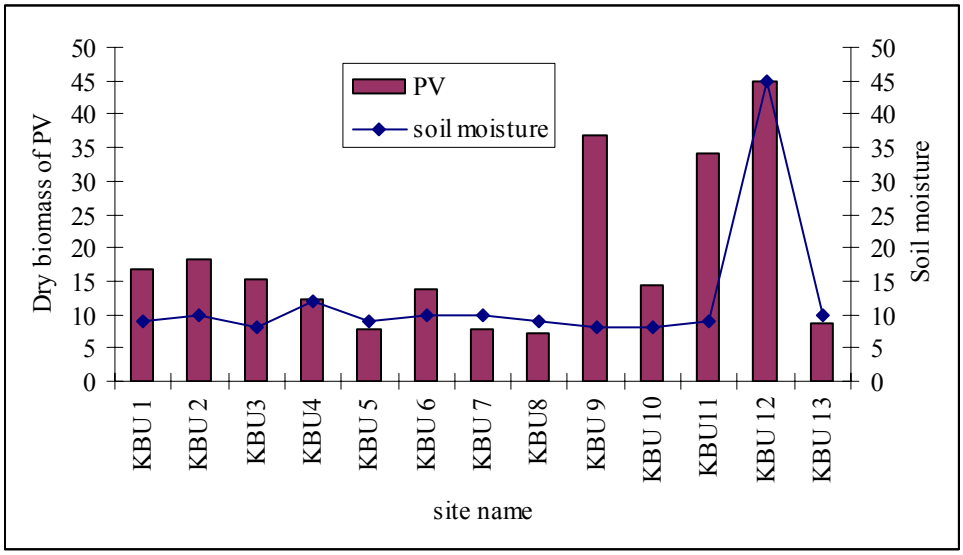

b)

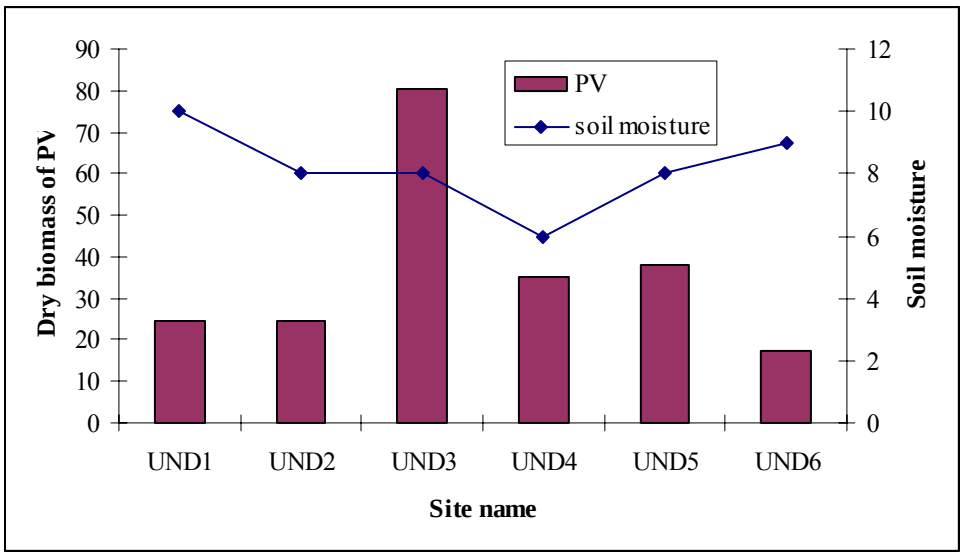

Figure 11 The dynamics of soil moisture and dry biomass of photosynthetic vegetation. From panels 3 (a) to (d) are those derived from semiarid area and panels (e) and (f) shows those in arid area. Site name listed in abbreviation of site name Table 1. a) KBU site and b) UND site

c)

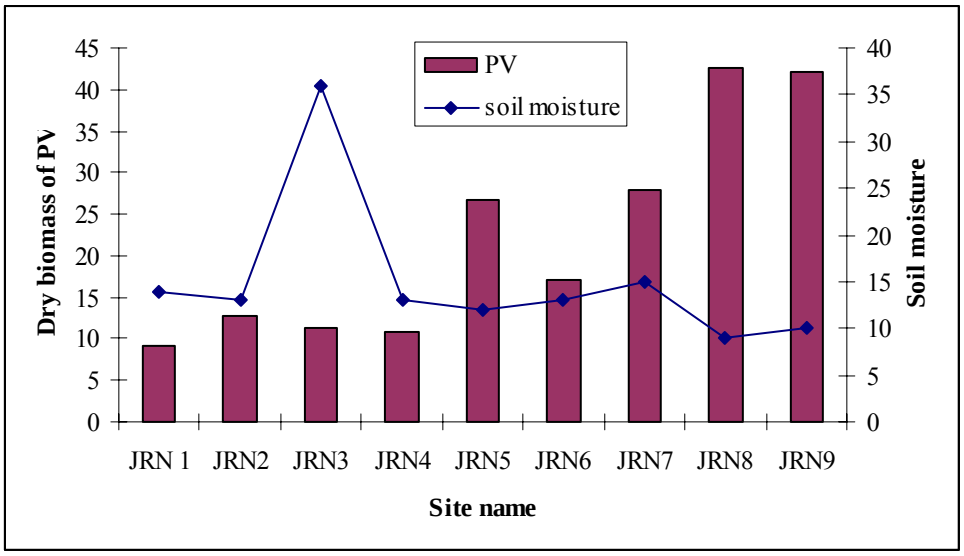

d)

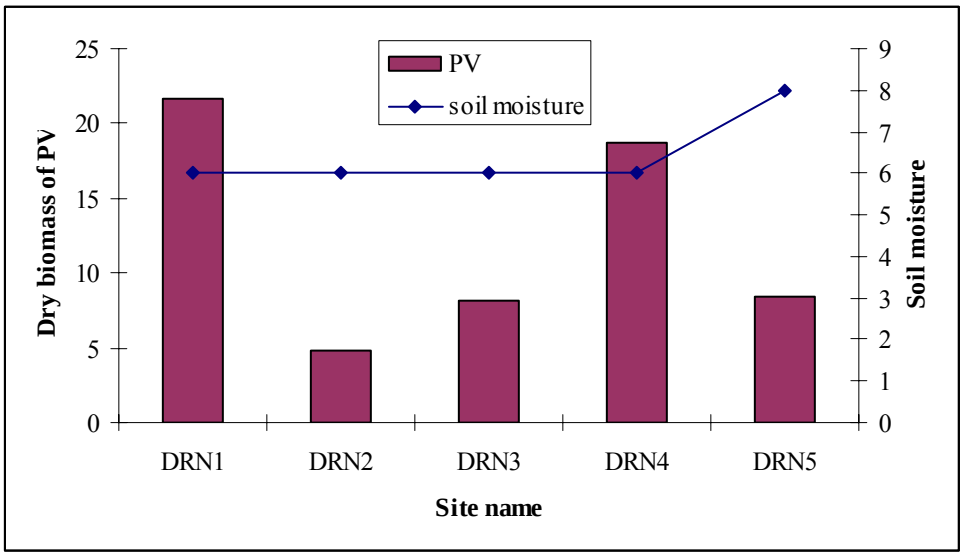

Figure 11 The dynamics of soil moisture and dry biomass of photosynthetic vegetation. From panels 3 (a) to (d) are those derived from semiarid area and panels (e) and (f) shows those in arid area. Site name listed in abbreviation of site name Table 1. c) JRN site and d) DRN site

e)

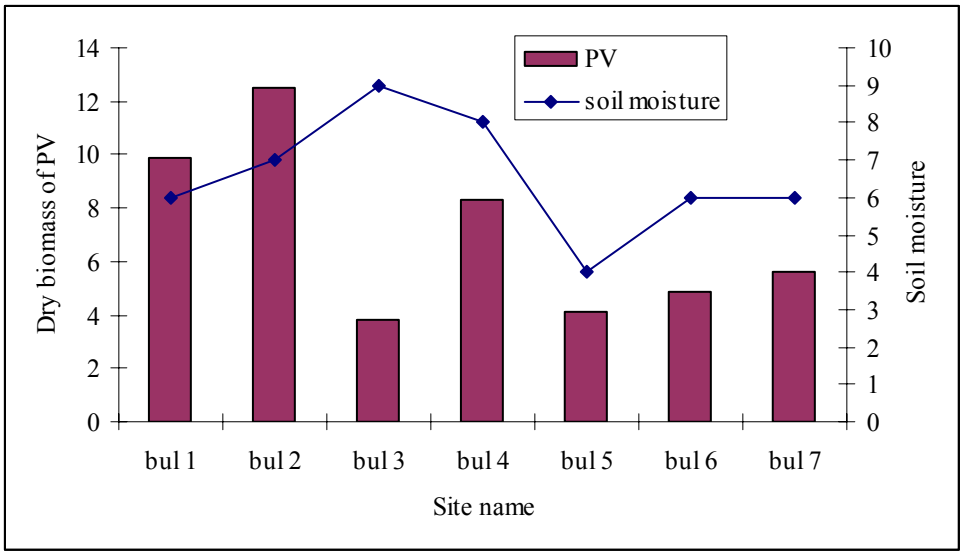

f)

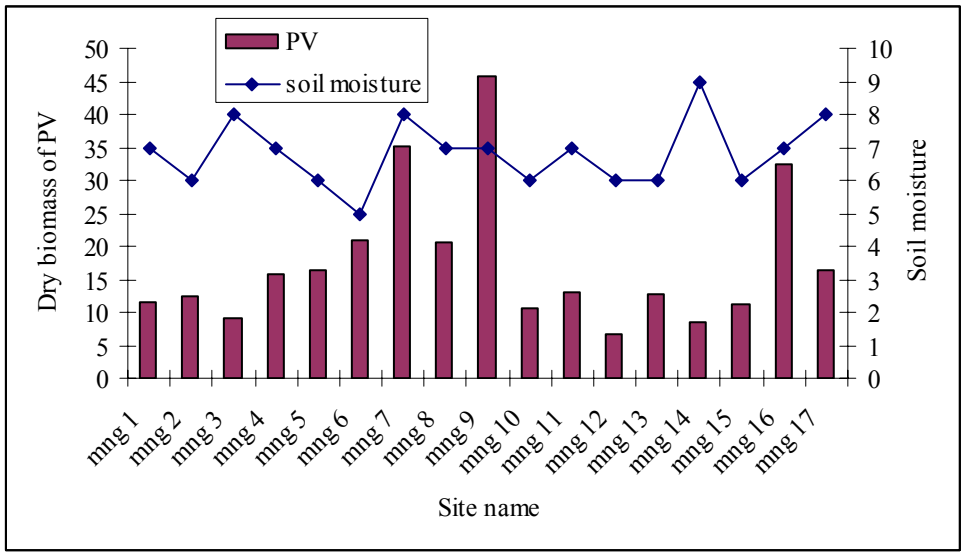

Figure 11 The dynamics of soil moisture and dry biomass of photosynthetic vegetation. From panels 3 (a) to (d) are those derived from semiarid area and panels (e) and (f) shows those in arid area. Site name listed in abbreviation of site name Table 1.

3-3 Analysis of spectral shape

A field spectral dataset of PV, NPV, and bare soils was complied for 50 semiarid and arid sites in eastern steppe and Gobi steppe of Mongolia, representing wide type of data structure of plant species, vegetation conditions, and soil properties. Reflectance of dominant PV and bare soil collected at 50 semiarid and arid sites in eastern steppe and Gobi steppe regions of Mongolia are shown in Figures 12 and 13. You can see from Figure 10 that PV reflectance varied the most in the near infrared region (NIR) between 700 nm and 1300 nm and the least in the SWIR region. The spectral reflectance of PV is much difference in NIR due to the PV biomass of each observed site. Indeed, the spectral reflectance of PV of green band is higher than that of red and blue bands. As the growing plants turn green in color, the chlorophyll in the leaves absorbs the red radiation and at the same time increases the blue reflectance. It is required for photosynthesis process. Nonphotosynthetic vegetation and bare soil reflectance was most variable in the SWIR region from 1300 to 2500 nm, however, the most consistent spectral region was SWIR2 from 2100 to 2400 nm in Figure 13.

Figure 13 shows the spectral reflectance of soil figure. Due to the moisture that is contained in the plant there is a steep decline in 1350-1400 nm and 1800-2000nm wavelength. Figure 14 and 15 shows reflectance of PV and bare soil in SWIR region. This is indicating that SWIR2 region is give almost consistent reflectance both of PV and bare soil.

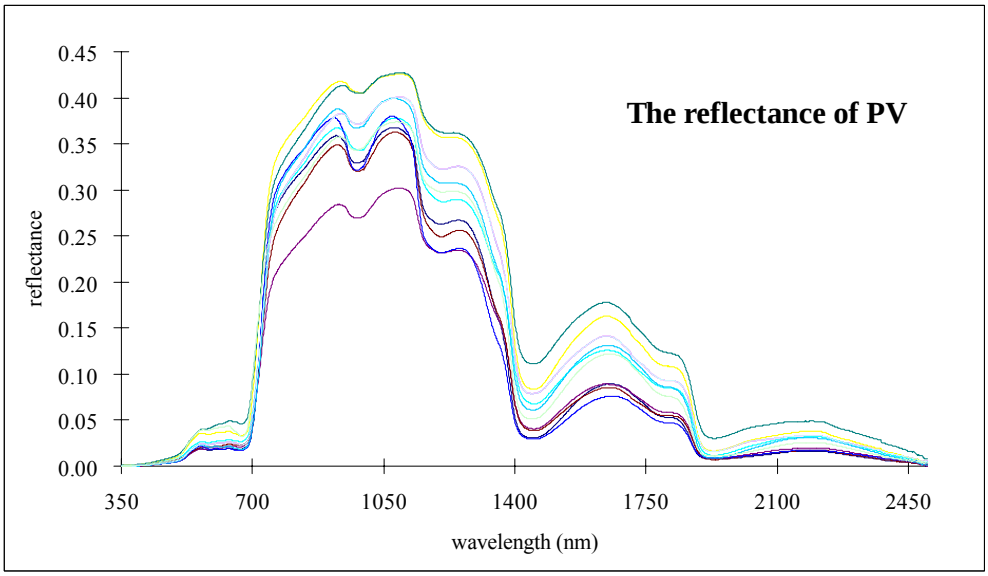

Figure 12 The reflectance of photosynthetic vegetation collected at semiarid and arid area of Mongolia. Full range of variability is shown.

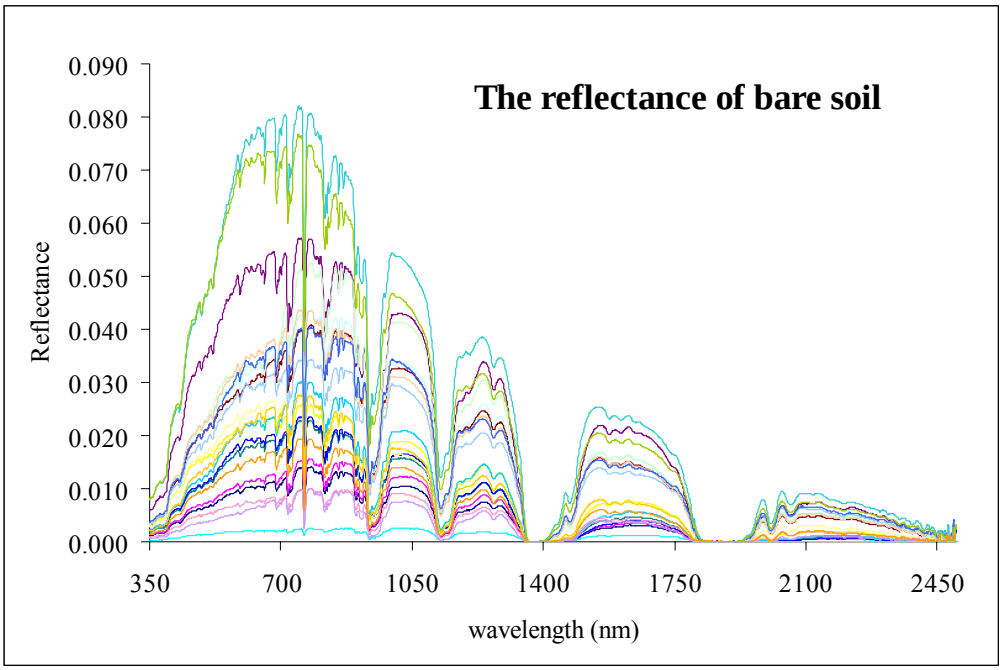

Figure 13 The reflectance of all 50 samples of bare soil collected at semiarid and arid area of Mongolia. Full range of variability is shown.

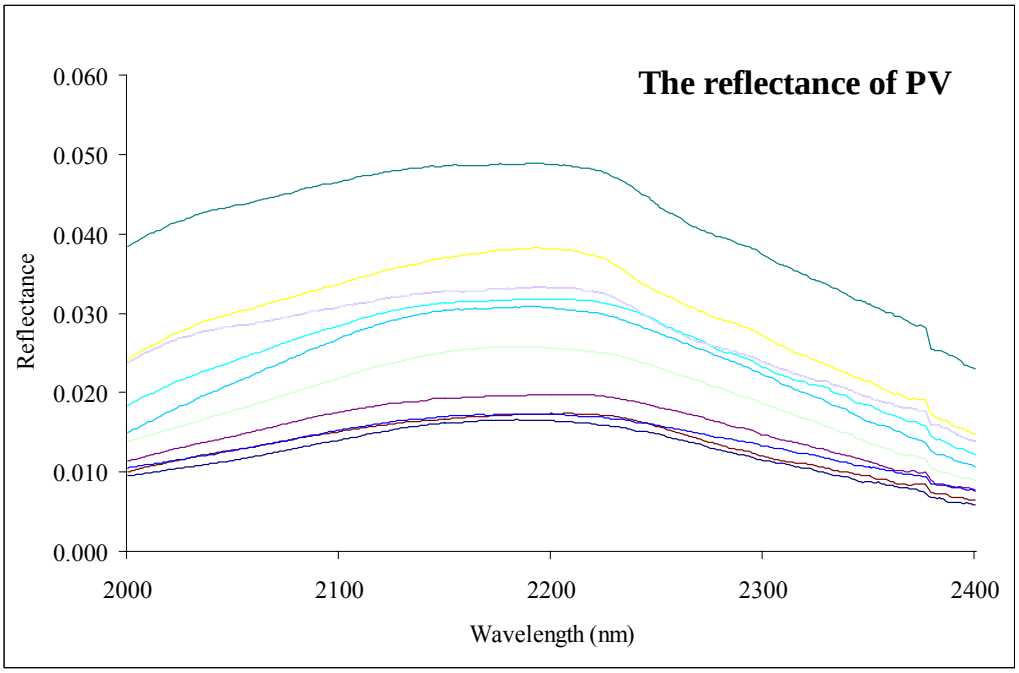

Figure 14 The reflectance of photosynthetic vegetation in SWIR spectral region is shown.

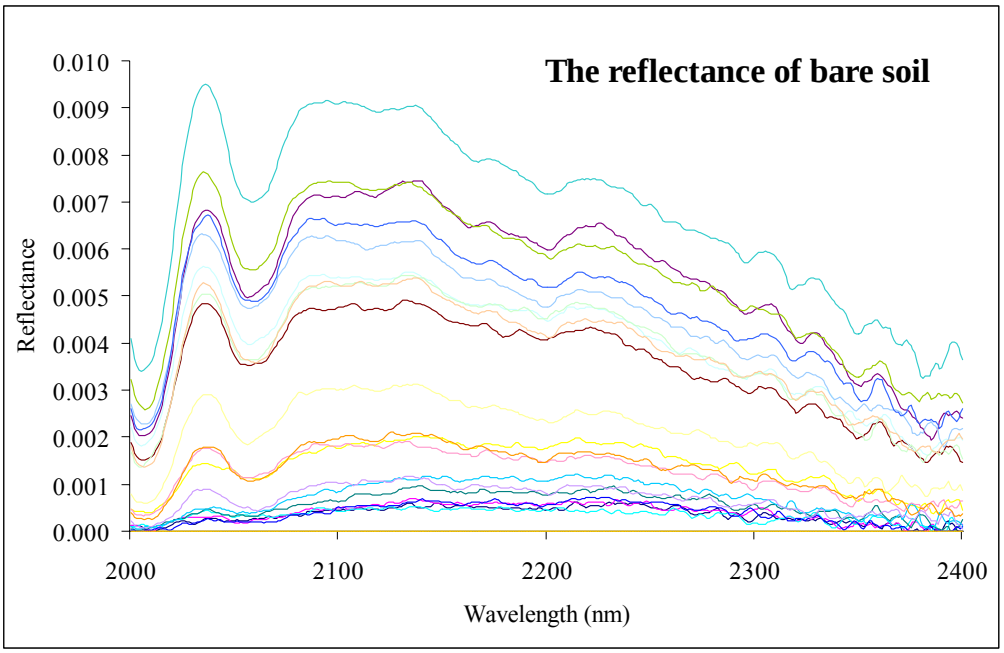

Figure 15 The reflectance of bare soil in SWIR spectral region is shown.

However, within our field sites, there is stable reflectance for PV, NPV, and bare soil in the SWIR2 region from 2100 nm to 2400 nm in Figure 16.

Therefore, we reanalyzed to find which wavelength of the SWIR region is most appropriate for spectral unmixing model using endmember sets. High frequency filtering and linear transformation to emphasize spectral shape were used and this includes two possibilities for characterizing spectral shapes, i.e., “DERIVATIVE” spectra and “TIED” spectra, with the latter defined as subtracting the value at one wavelength from other wavelengths. This is the tied point.

Figures 17-20 show that within the SWIR region, there is most stable reflectance for PV, NPV, and bare soils in from 2075 nm to 2275 nm wavelength region in tied spectra. In the case of derivative reflectance, its shape is variable in SWIR region.

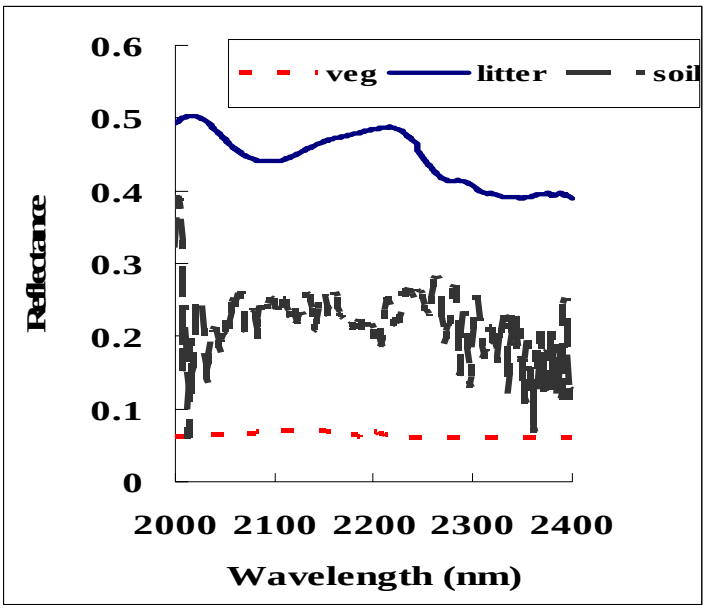

Figure 16. Typical reflectance of PV (dotted), NPV (solid), and bare soil (dashed) in SWIR region

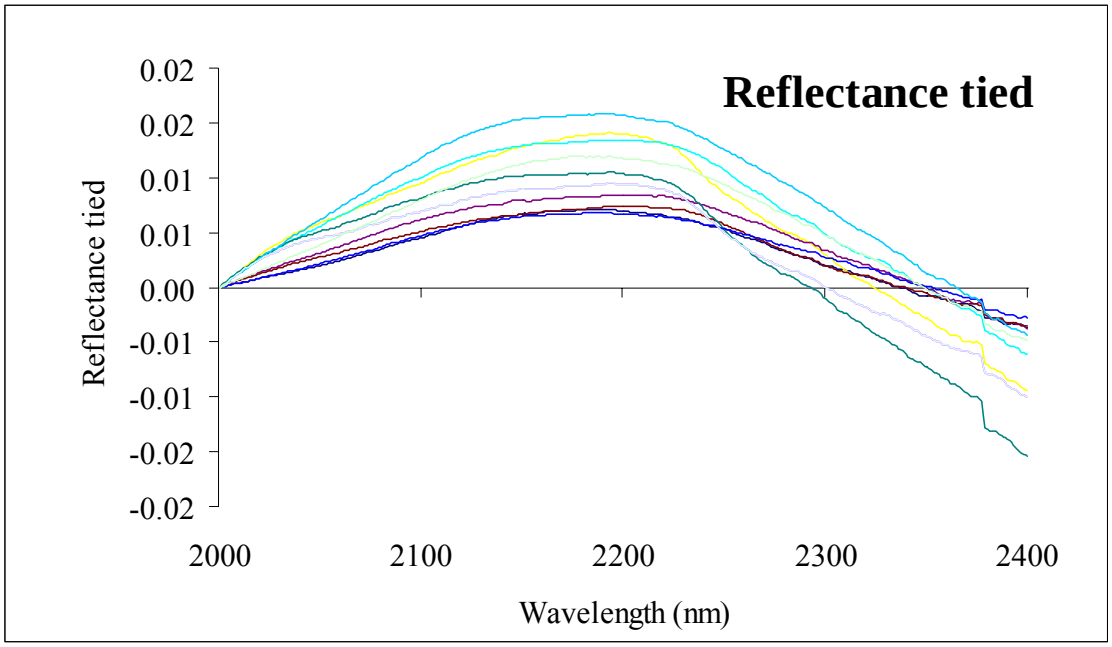

Figure 17. The tied reflectance of photosynthetic vegetation collected at semiarid and arid area of Mongolia. SWIR range of variability is shown.

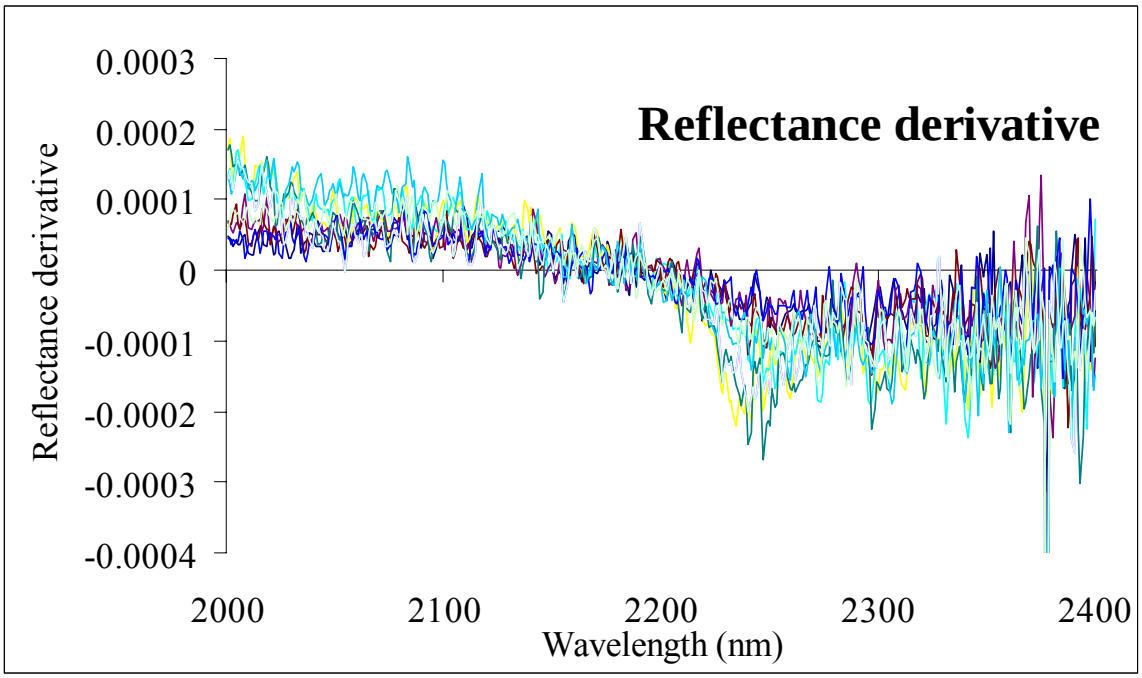

Figure 18 The derivative reflectance of photosynthetic vegetation collected at semiarid and arid area of Mongolia. SWIR range of variability is shown.

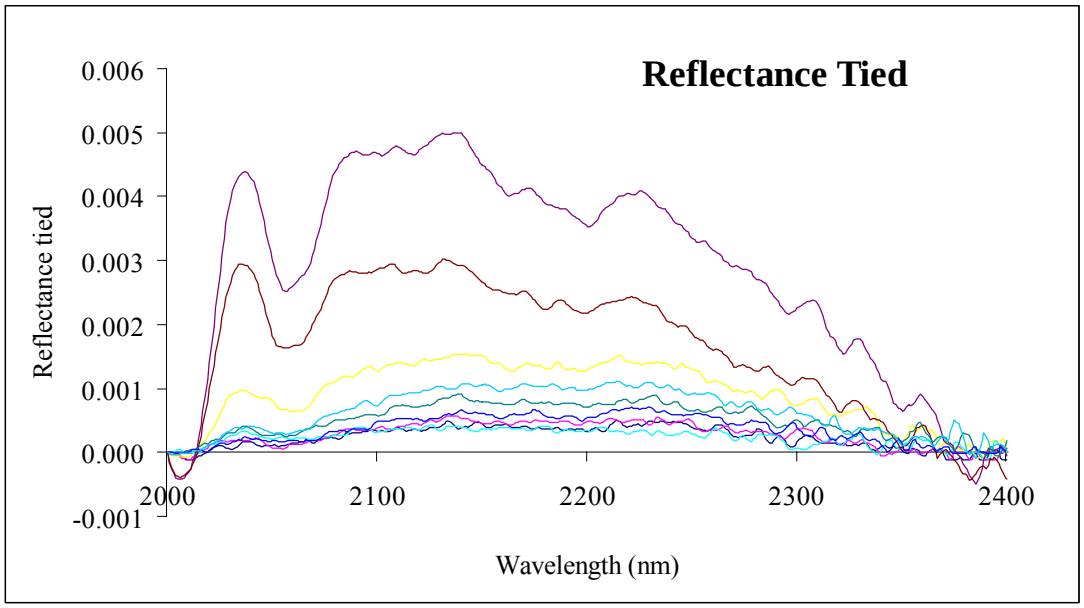

Figure 19 The tied reflectance of bare soil collected at semiarid and arid area of Mongolia. SWIR range of variability is shown.

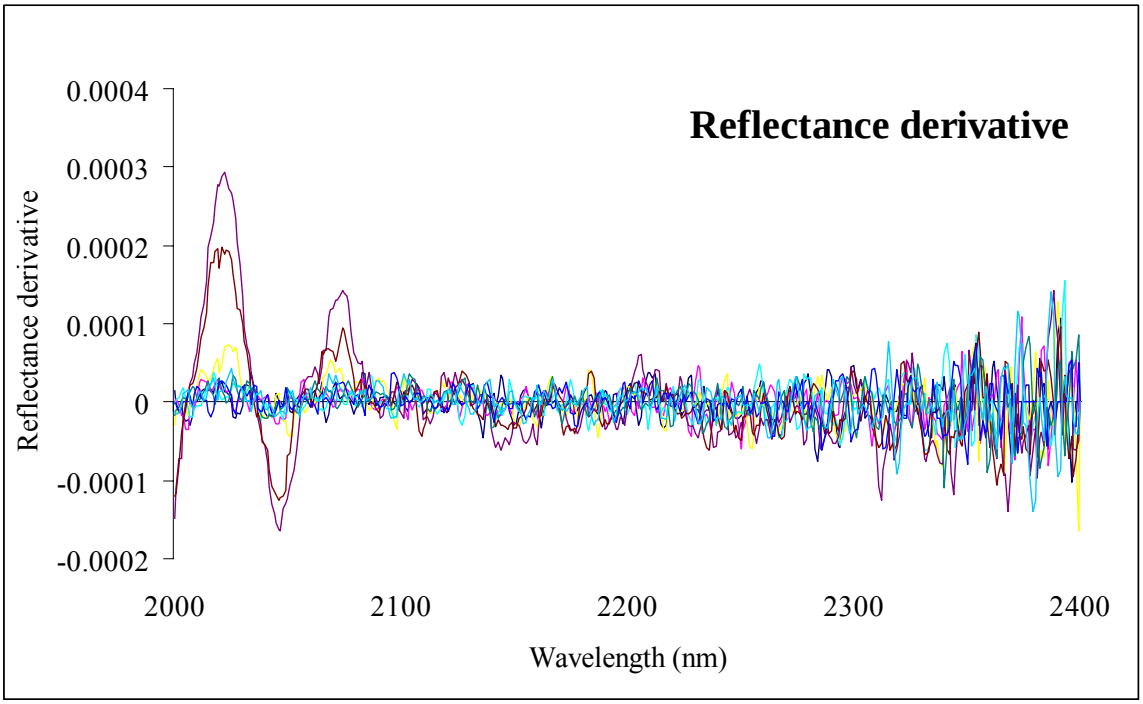

Figure 20 The derivative reflectance of bare soil collected at semiarid and arid area of Mongolia. SWIR range of variability is shown.

3-4. Effect of noise on cover fractions

This study investigated the effects of varying noise levels on the MCU-derived fractions using both derivatives and tied spectra. Normally distributed noise with mean of zero and standard deviation ranging from 0% to 15% of the signal was added to each of modeled spectra. The MCU procedure was then performed on each simulated spectrum using 100 endmember-database runs in the from 2075 nm to 2275 nm wavelength interval. As can be seen in Table 5, in baseline case from 0% noise to 5% noise level, both tied and derivative spectra returned accurate fractions for each modeled true value. However, the tied spectra are much less sensitive to the noise as compared to the derivative spectra. Indeed, when the modeled true values are 40% of PV, 55% of NPV, and 5% of bare soil, calculated PV was 16%, and NPV was 78 % at 10% noise level, and the calculated bare soil was 7% at 15 % noise level using derivative spectra. As a result, the tied spectra were judged more reliable for spectral unmixing model to determine LCFs in this study area than the derivative spectra because tied spectra were much less susceptible to noise in comparison to the derivative. Therefore, the tied SWIR spectra were adopted for use in all subsequent unmixing applications. The cover fractions resulting from Monte Carlo technique procedure invariability had normal distribution in each pixel. Therefore, we used mean to estimate the cover fractions and the standard deviation to form confidence interval for the true fraction.

Monte Carlo technique has been popular due to their simplicity and interpretability, but they can be cumbersome if too much iteration is required to develop confident statistics. In this situation, an important factor to consider is the minimum number of inversions or runs, in the SUM needed to converge to give the mean and standard deviation. Figure 21 shows the calculated mean and standard deviations from MCU performed with varying number of runs on spectrum modeled from different fractions of each endmember. This result suggests that additional runs beyond 40 have

little effect on derived fractions. Therefore, a conservative value of 50 runs was thus chosen for the remainder of the study.

Table 5 Effects of noise on calculated cover fractions using tied and derivative spectra.

Noise level	PV fraction		NPV fraction		Soil fraction	
%	Tied	Derivative	Tied	Derivative	Tied	Derivative
0	0.40	0.39	0.54	0.54	0.04	0.04
5	0.39	0.38	0.54	0.57	0.05	0.06
10	0.38	0.16	0.53	0.78	0.04	0.04
15	0.39	0.31	0.54	0.53	0.04	0.07
Model fractions	PV=0.4		NPV=0.55		Soil=0.05	

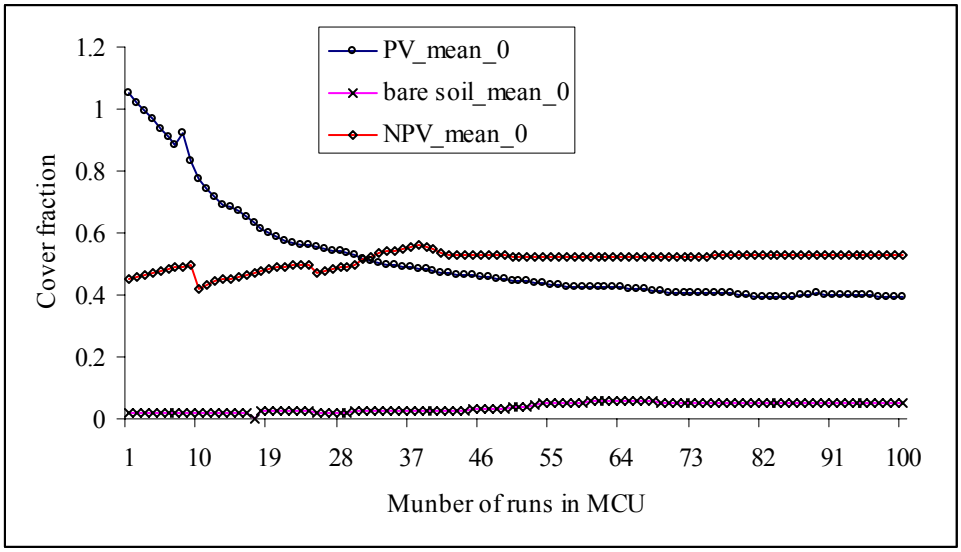

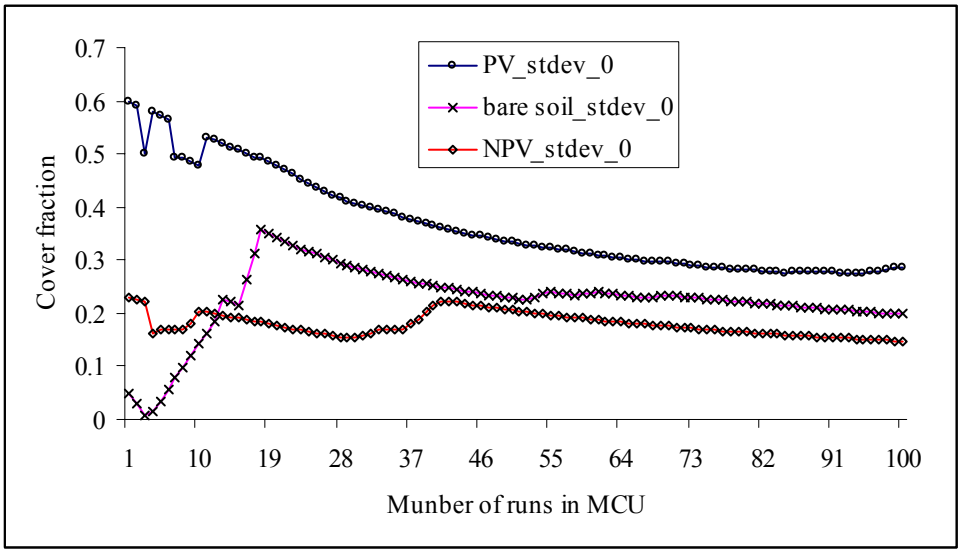

Figure 21 Mean and standard deviation of each endmember fractions number of runs in MCU procedure.

3-5. Bi-directional reflectance correction

We carried out bi-directional reflectance spectrometry from land cover type's community in the field sites, which includes 24 effective series of data from semiarid area in 2005 and 26 series of data in 2006 from arid area of Mongolia. The bidirectional reflectance distribution function model was used to correct spectral reflectance data from field with field bidirectional reflectance data derived from semiarid and arid area. The performance is indicated with solar azimuth at 0° and elevation angle at 30° in Figure 22. As can be seen in figure 20, the bidirectional reflectance distribution curve and comparison between predicted and observed reflectance values are shown in the SWIR spectral region. From top side, panel (a) shows semiarid area and panel (b) present to arid area. Also you can see that, both in semiarid and arid area, a good agreement between predicted and observed reflectance values in the SWIR spectral region was obtained. This, results suggest that the bidirectional reflectance distribution function model can work on SWIR spectral region. Therefore corrected reflectance data, calculates by bidirectional reflectance distribution function model can be used for spectral unmixing approach for land cover fractions.

a)

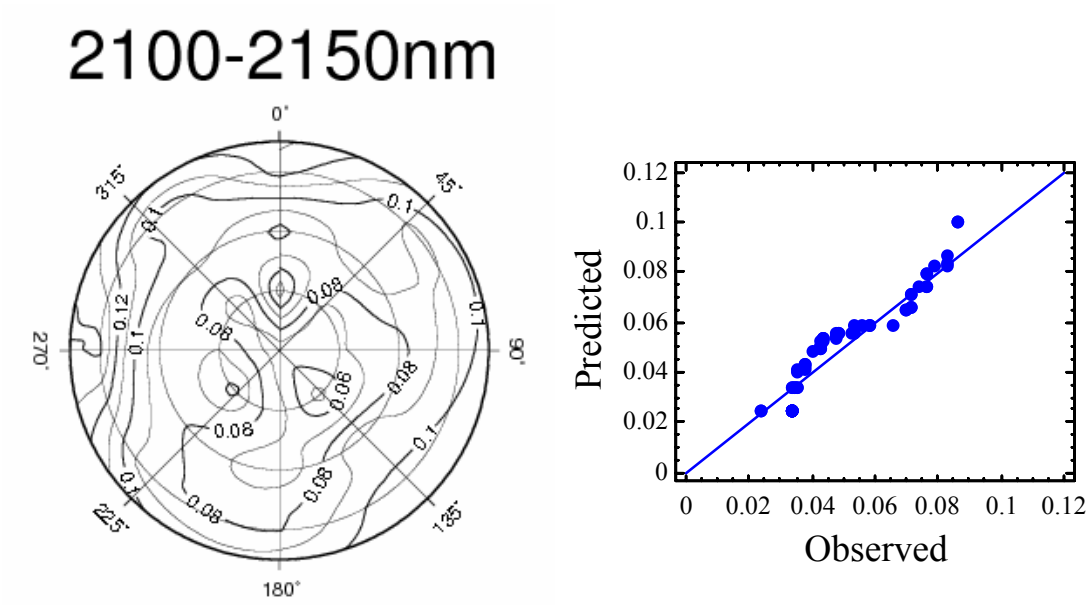

b)

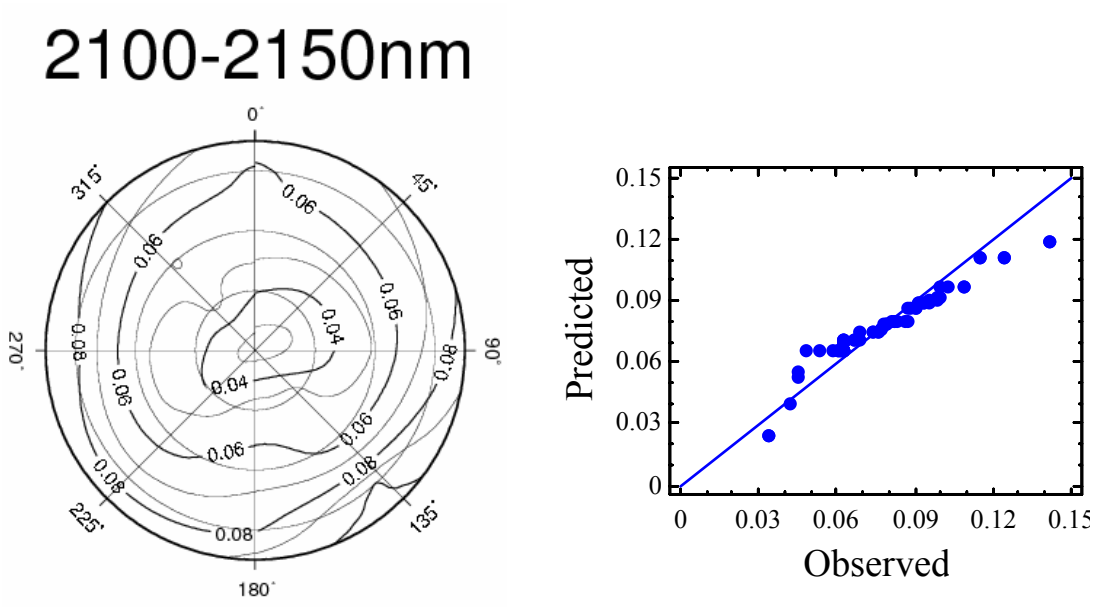

Figure 22 Bi-Directional Reflectance Distribution curve and comparison between predicted and observed reflectance values on the SWIR spectral region. Semiarid (a), and Arid (b).

3-6. Derived Land covers fractions from spectral unmixing approach

We tried to determine regional scales LCFs of semiarid and arid area in Mongolia using reflectance signature from SWIR region, calculated by spectral unmixing approach including Monte Carlo analysis. We had investigated to collect field measurement data from many different locations within both of semiarid and arid area, which can be indicated environmental condition and vegetation transit of semiarid and arid ecosystems of Mongolia. Therefore, final results of the determined land cover fractions should be represented, that is environmental characteristics of the regional ecosystems. The spectral unmixing model is performed with randomly selected spectra reflectance of each endmember bundle from tied spectra data set and spectral data of pixel reflectance including all endmember information. In our study, we used correction for field reflectance data using BRDF and then outcomes of BRDF give pixel reflectance data at different viewing angles (30°, 50° and 70°). Using these pixel reflectance data, we applied to spectral unmixing model and land cover fractions were determined. In semiarid area, PV spectra bundle derived from *Stipa Krylovii* Roshev, which widely distributed vegetation within semiarid area and *Allium Mongolicum* vegetation was used in arid area. However, use of different species as the PV endmember did not change the final results as we tested widely distributed 2 kind of vegetation species derived from study area.

Additionally, we compared derived land cover fractions from different viewing angles (30°, 50° and 70°). The result is summarized as statistics and correlations matrix. (Table 6 - 8).

As can be seen in Table 6, correlations between each pair of variables are shown. These correlation coefficients range between -1 and +1 and measure the strength of the linear relationship between the variables. Also shown in parentheses is the number of pairs of data values used to compute each coefficient. The second number in each location of the table is a P-value which tests the statistical significance of the estimated

correlations. P-values below 0.05 indicate statistically significant non-zero correlations at the 95% confidence level.

Table 7 and 8 shows summary statistics for each of the calculated land cover fractions value variables at different viewing angle.

The performance is indicated in Figures 23-25. Comparison of calculated each endmember's fractions values and actual values agree equally well with each other for three view angles. These results suggest that we can use any angles as input to the spectral unmixing model to estimate land cover fractions value in arid and semiarid region of Mongolia. Moreover, use of different species as the PV endmember bundles did not appreciable change the final results as we tested widely distributed two kinds of vegetation species derived from study area.

a)

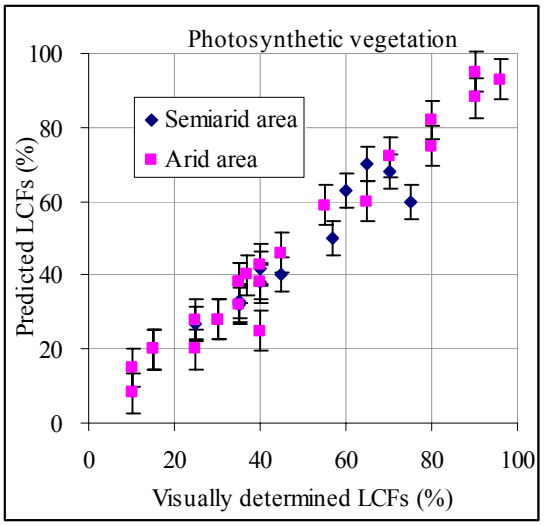

b)

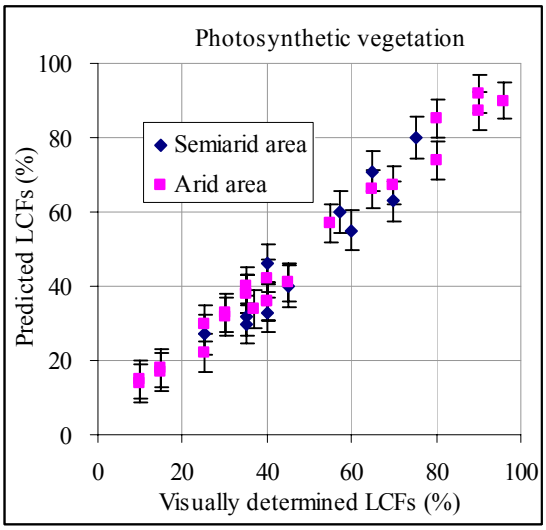

c)

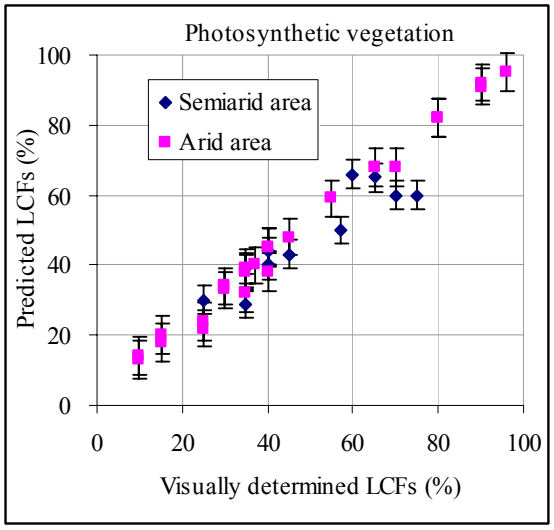

Figure 23 Comparison of the predicted photosynthetic vegetation values calculated by SUM and visually determined photosynthetic vegetation values. Panel (a) is derived from sensor viewing angle was 30°, panel (b) is derived from sensor viewing angle was 50° and panel (c) is derived from sensor viewing angle was 70° .Both results of semiarid and arid area are shown.

a)

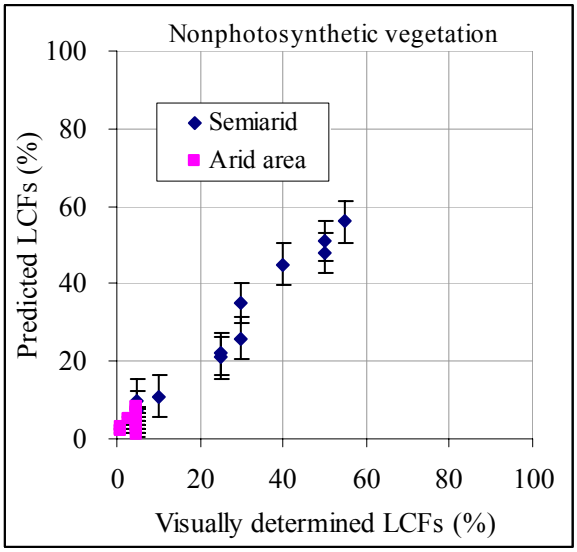

b)

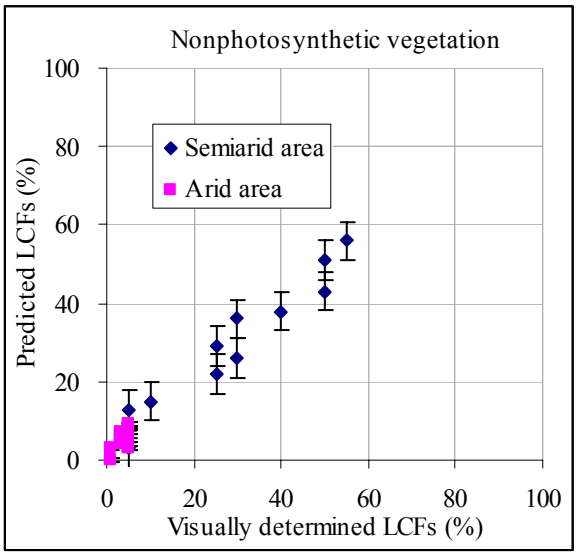

c)

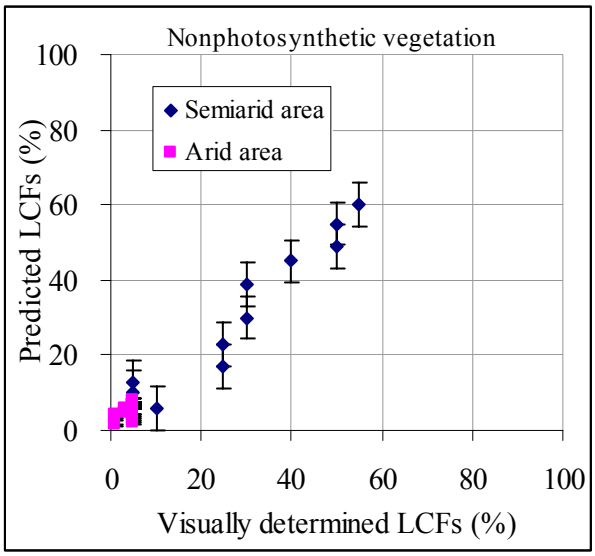

Figure 24 Comparison of the predicted nonphotosynthetic vegetation values calculated by SUM and visually determined nonphotosynthetic vegetation values. Panel (a) is derived from sensor viewing angle was 30°, panel (b) is derived from sensor viewing angle was 50° and panel (c) is derived from sensor viewing angle was 70° .Both results of semiarid and arid area are shown.

a)

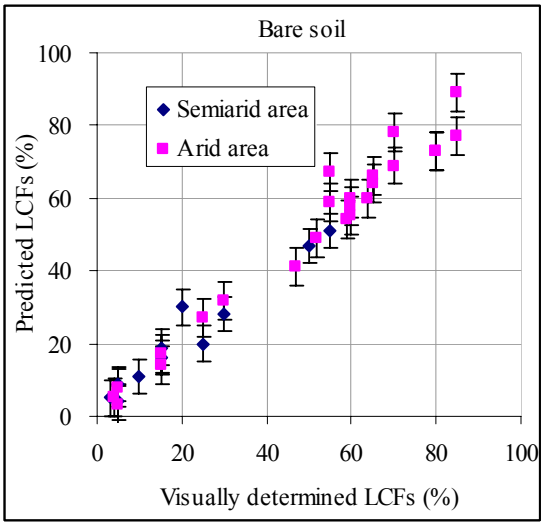

b)

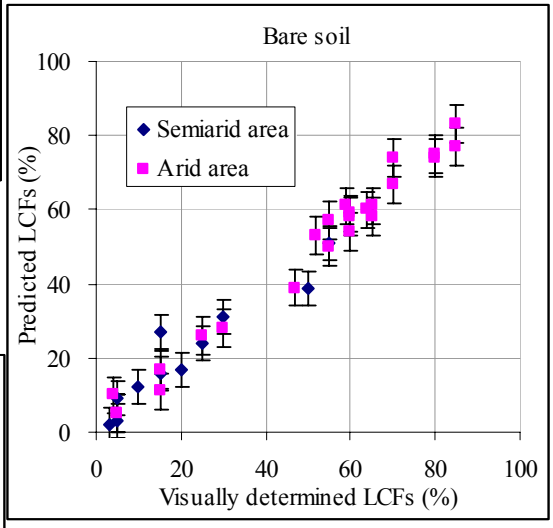

c)

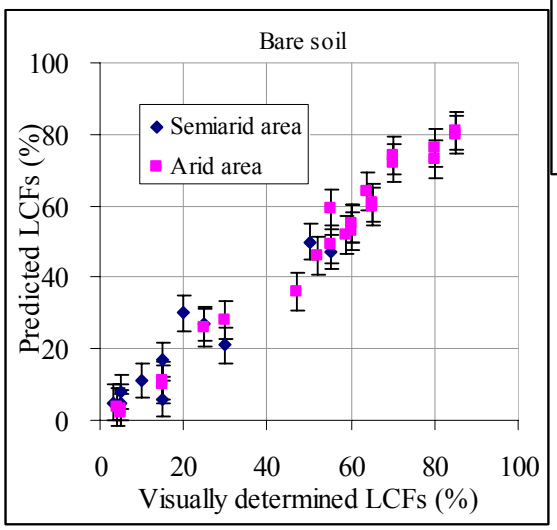

Figure 25 Comparison of predicted bare soil values calculated by SUM and visually determined bare soil values. Panel (a) is derived from sensor viewing angle was 30°, panel (b) is derived from sensor viewing angle was 50° and panel (c) is derived from sensor viewing angle was 70° .Both results of semiarid and arid area are shown.

Table 6 Correlation matrixes of derived land cover fractions from different viewing angle.

Semiarid area	View angle	PV by VD	NPV by VD	BS by VD	Arid area	View angle	PV by VD	NPV by VD	BS by VD
PV by SUM	30 degree	0.940 0.000			PV by SUM	30 degree	0.984 0.000		
PV by SUM	50 degree	0.927 0.000			PV by SUM	50 degree	0.997 0.000		
PV by SUM	70 degree	0.915 0.001			PV by SUM	70 degree	0.995 0.001		
NPV by SUM	30 degree		0.980 0.000		NPV by SUM	30 degree		0.561 0.003	
NPV by SUM	50 degree		0.966 0.000		NPV by SUM	50 degree		0.6649 0.001	
NPV by SUM	70 degree		0.960 0.000		NPV by SUM	70 degree		0.560 0.004	
BS by SUM	30 degree			0.9722 0.000	BS by SUM	30 degree			0.982 0.000
BS by SUM	50 degree			0.9521 0.000	BS by SUM	50 degree			0.990 0.000
BS by SUM	70 degree			0.9435 0.000	BS by SUM	70 degree			0.990 0.000

Correlation

P-value

PV= photosynthesis vegetation

NPV= nonphotosynthesis vegetation

BS= bare soil

VD= visually determined,

SUM= spectral unmixing model

Table 7 Summary statistics of derived land cover fractions from different viewing angle in semiarid area.

	PV by VD	NPV by VD	BS by VD
Average	49.72	29.54	21.18
Minimum	25.0	5.0	3.0
Maximum	75.0	55.0	55.0
Range	50.0	50.0	52.0
View angle=30°	PV by SUM	NPV by SUM	BS by SUM
Average	47.54	30.18	21.81
Variance	2.37	3.14	2.51
Standard deviation	0.15	0.17	0.15
Minimum	27.0	7.0	4.0
Maximum	70.0	56.0	51.0
Range	43.0	49.0	47.0
View angle=50°	PV by SUM	NPV by SUM	BS by SUM
Average	48.81	30.18	21.0
Variance	3.27	2.70	2.32
Standard deviation	0.18	0.16	0.15
Minimum	27.0	3.0	2.0
Maximum	80.0	56.0	51.0
Range	53.0	53.0	49.0
View angle=70°	PV by SUM	NPV by SUM	BS by SUM
Average	47.8182	31.54	20.63
Variance	1.77	3.64	2.65
Standard deviation	0.13	0.19	0.16
Minimum	29.0	6.0	5.0
Maximum	66.0	60.0	50.0
Range	37.0	54.0	45.0

PV= photosynthesis vegetation, NPV= nonphotosynthesis vegetation, BS= bare soil, VD= visually determined, SUM= spectral unmixing model, 30, 50 and 70= viewing angle

Table 8 Summary statistics of derived land cover fractions from different viewing angle in arid area.

	PV by VD	NPV by VD	BS by VD
Average	45.54	4.25	50.45
Minimum	10.0	1.0	4.0
Maximum	96.0	5.0	85.0
Range	86.0	4.0	81.0
View angle=30°	PV by SUM	NPV by SUM	BS by SUM
Average	45.45	4.75	49.9167
Variance	6.89	0.05	6.47
Standard deviation	0.26	0.02	0.25
Minimum	8.0	1.0	3.0
Maximum	95.0	8.0	89.0
Range	87.0	7.0	86.0
View angle=50°	PV by SUM	NPV by SUM	BS by SUM
Average	46.0	5.58	48.41
Variance	6.24	0.07	6.03
Standard deviation	0.24	0.03	0.25
Minimum	14.0	0.0	5.0
Maximum	92.0	9.0	83.0
Range	78.0	9.0	78.0
View angle=70°	PV by SUM	NPV by SUM	BS by SUM
Average	47.5	5.43	47.06
Variance	6.77	0.02	6.76
Standard deviation	0.26	0.01	0.26
Minimum	13.0	1.5	2.0
Maximum	95.0	8.0	81.0
Range	82.0	6.5	79.0

PV= photosynthesis vegetation, NPV= nonphotosynthesis vegetation, BS= bare soil, VD= visually determined, SUM= spectral unmixing model, 30, 50 and 70= viewing angle

3-7 Derived Land covers fractions from supervised classification method

The image should be scanned accordingly and the image elements representing true LCFs can be calculated as percentage of total image elements. Then the result obtained being the final LCFs. We show a result of the classification is presented in Figures 26-27 with classified percentage of LCFs at KBU 1 site from semiarid area and MNG1 site from arid area. Panel (a) shows digital camera image of real land cover fractions at field site. The panel (b) shows IHS components on digital camera image transformed from RGB color image to IHS color image using a color space-transformation method of ERDAS imagine. The panel (c) shows classified image using the supervised classification method. When panel (c) is compared with the original digital images (panel (a)), the results can included some disadvantages, (i) in the case of bare soil, in the shadow areas can be determined accurately as bare soil, and (iii) another possibility for mistaking photosynthetic vegetation cover in the shadow as bare soil is quit high, and this inaccurate determination may lead to the results of LCFs.

In Figures 28-30 show comparison between classified LCFs values and visually determined LFCs values in semiarid and arid area of Mongolia. These comparison results indicate that calculated photosynthetic vegetation (Figure 28) and nonphotosynthetic vegetation (Figure 29) values and visually determined values agree with each other. But in the case of bare soil (Figure 30), calculated bare soil values and visually determined values bad agree with each other. Because the results of the supervised classification method was included, if two different objectives are close enough (i.e. bare soil and shadow); it combine these two objectives into one objective. Thus, final results were being obtained larger than the true value.

a)

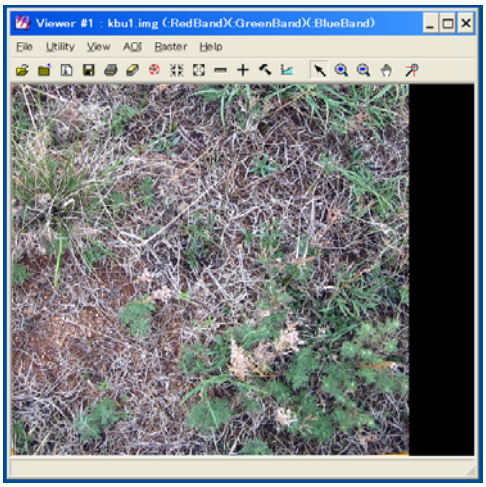

b)

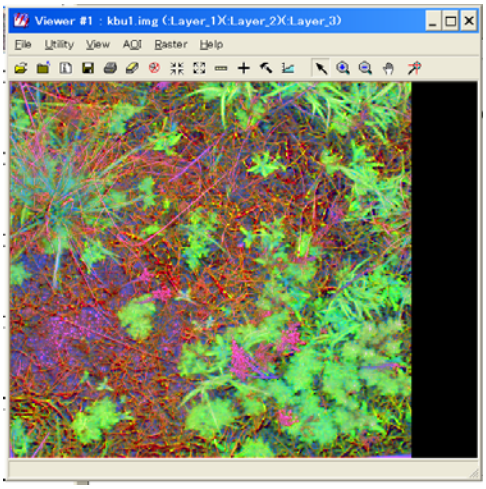

c)

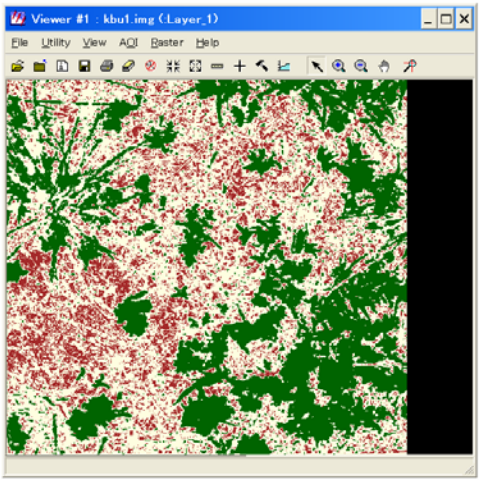

Figure 26 Typical LCFs at KBU site 1 in semiarid area. Top side panel (a) shows digital camera image of KBU 1; panel (b) shows image is transformed IHS color image from RGB color image; and panel (c) shows classified image using supervised classification method.

a)

b)

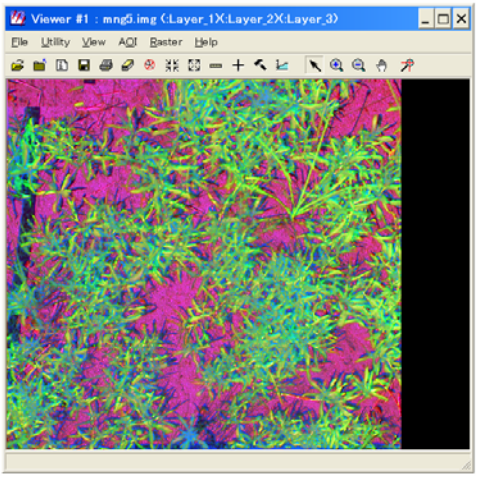

c)

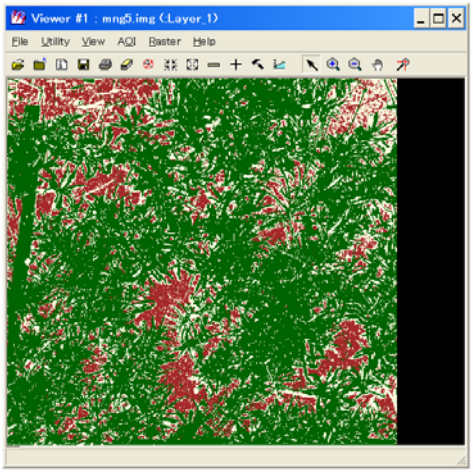

Figure 27 Typical LCFs at MNG site 1 in arid area. Top side panel (a) shows digital camera image of MNG 1; panel (b) shows image is transformed IHS color image from RGB color image; and panel (c) shows classified image using supervised classification method.

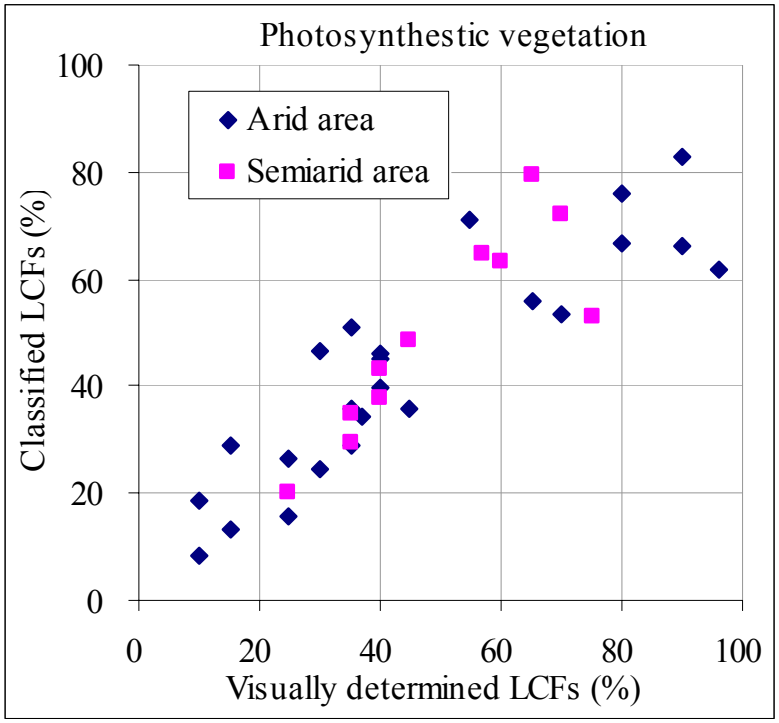

Figure 28 Comparison of the predicted photosynthetic vegetation values calculated by supervised classification method and visually determined photosynthetic vegetation values. Both results of semiarid and arid areas are shown

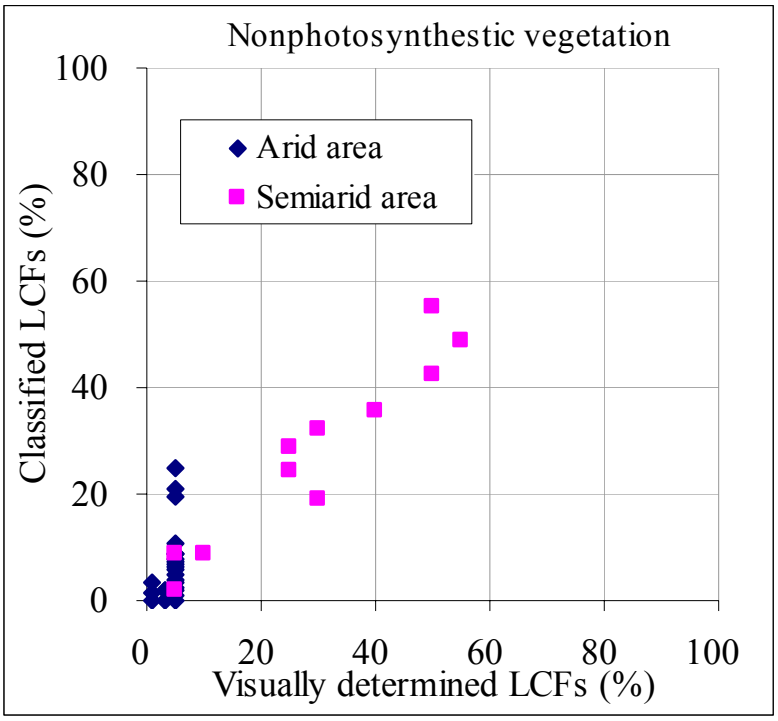

Figure 29 Comparison of predicted nonphotosynthetic vegetation values calculated by supervised classification method and visually determined nonphotosynthetic vegetation values. Both results of semiarid and arid areas are shown

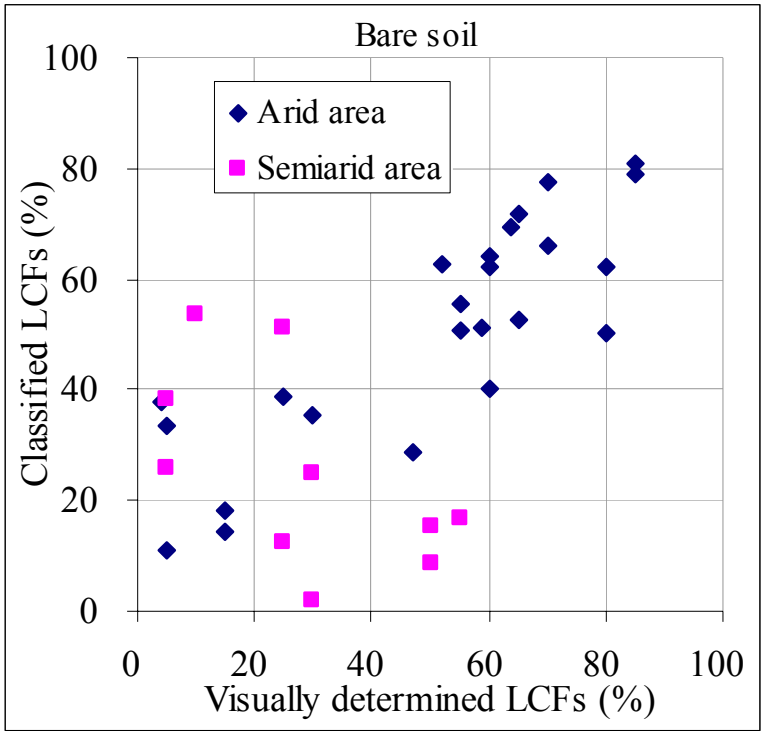

Figure 30 Comparison of the predicted bare soil values calculated by supervised classification method and visually determined bare soil values. Both results of semiarid and arid areas are shown

3-8 Relationship between visually determined LCFs and different model results

In this present study, we shows calculated the land cover fractions values using various methods was evaluated quantitatively and compared. During the statistic analysis process, the following indices were considered.

$$RMS = \sqrt{\frac{1}{n}\sum_{i=1}^{n} X_i^2} \qquad (9)$$

where *RMS* is root mean square error, *Xi* represented results obtained using various method. The results are presented in Table 10.

Also we have checked relationship between visually determined land cover fractions and different model results using correlation analysis.

As can be seen in table 9, both SUM and SCM have good relationship with visually determined true values. However, SUM is better than SCM to calculate the LCFs. The following correlation analysis can be summarized as follows: SUM (R=0.98) > SCM (R=0.88) for PV, SUM (R=0.5) > SCM (R=0.4) for NPV and SUM (R=0.93) > SCM (R=0.80) for bare soil. As can be seen in table 6, RMSE of supervised classification method is less than the spectral unmixing model in arid area. RMSE of the supervised classification method is more than spectral unmixing model in semiarid area. These results confirm that the spectral unmixing model including Monte Carlo analysis has the highest accuracy for estimation of LCFs.

Table 9 Correlation coefficients of estimating LCFs from different methods

PV	Visual	SUM	SCM
Visual	1		
SUM	0.98	1	
SCM	0.88	0.80	1

NPV	Visual	SUM	SCM
Visual	1		
SUM	0.5	1	
SCM	0.4	0.3	1

Bare soil	Visual	SUM	SCM
Visual	1		
SUM	0.93	1	
SCM	0.80	0.75	1

Table 10 RMSE of estimating LCFs from different methods

Arid			
	PV	NPV	Bare soil
SCM	0.47	0.09	0.54
SUM	0.52	0.05	0.56
Semiarid			
	PV	NPV	Bare soil
SCM	0.53	0.32	0.29
SUM	0.50	0.35	0.27

Conclusions

We used various methods for estimate land cover fractions of semiarid and arid ecosystems Mongolia. First, we applied a spectral unmixing model using field spectral measurements data to investigate and collected from those ecosystems. Second, also we applied supervised classification method using digital camera image to calculate land cover fractions in semiarid and arid area of Mongolia with "ERDAS IMAGINE" (Leica Geosystems, Geospatial Imaging, LLC version 9.0 image processing software. The results of comparison of classified land cover fractions value and visually determined land cover fractions value are agreement for photosynthesis vegetation and non photosynthesis vegetation, but in bare soil the agreement is not as good. This was because image elements corresponding to bare soil can not be distinguished from image elements corresponding to shadow.

Thus, during this application of these methods of calculating land cover fractions, we can be concluded the following: (i) the bidirectional distribution function model can work in shortwave-infrared spectral region, as shown in figure 20. Quite high agreement between corrected spectral reflectance data and observed reflectance values in the shortwave-infrared spectral region was obtained in both of semiarid and arid area; (ii) conservative value of 50 runs number is enough in Monte Carlo analysis for calculating mean and standard deviations from Monte Carlo unmixing performed with varying number of runs on spectrum modeled from different fractions of each endmember, i.e. in Figure 19, additional runs beyond 40 have little effect on derived fractions. Large than 50 runs number have almost no effect on derived fractions; (iii) the accuracy of the supervised classification method is highly dependent on the section of specific area on image. The section of specific area is connecting with the identifying techniques of the

model and information of the data by user. Therefore, this method is highly dependent on the individual user; and (iv) when the data volume to be processed is significantly large, the supervised classification method requires a too much time and energy.

Finally, we investigated relationship between visually determined land cover fractions value and different model results. It can be seen that the correlation coefficient of land cover fractions calculations using visually determined and the different methods for determining the LCFs can be summarized as SUM (R=0.98) > SCM (R=0.88) for PV, SUM (R=0.5) > SCM (R=0.4) for NPV and SUM (R=0.93) > SCM (R=0.80) for bare soil. As shown in table 6, RMSE of supervised classification method is less than the spectral unmixing model in arid area and more than spectral unmixing model in semiarid area. These results confirm that the spectral unmixing model including Monte Carlo analysis has the highest accuracy for estimation of land cover fractions better than supervised classification method in study area. We believe still this analysis will serve as pilot information for further application in Mongolia. However, application of the spectral unmixing model needs further improvement and more data and some additional spectral measurements.

Acknowledgements

I would like to express my gratitude to Dr. M. Sugita Professor of Graduate School of Environmental Sciences, University of Tsukuba, and his endless attracting attentions during whole time, patience, enthusiasm, and guidance for my graduate work also for giving me many opportunities suggestions to field observation in Mongolia.

I would like to appreciate to Dr. D. Matsushima, associate professor of Chiba institute of Technology, for giving me inspiration for my research and providing access to the field spectral measurement, as well as bestowing upon me much of his time, patience, and expertise.

I am grateful to Dr. N. Tase and Dr. T. Tanaka, Professor of Graduate School of Environmental Sciences, University of Tsukuba, Dr. M. Tsujimura Assistant professor of Graduate School of Environmental Sciences, University of Tsukuba and Dr. T. Yamanaka Assistant professor of Terrestrial Environmental Research Center, University of Tsukuba for their countless suggestions, opportunity of plentiful discussions and guidance.

Also I am wishing to express my thanks to Dr. Ts. Adyasuren, president of Environmental Education and Research Institute of ECO ASIA, Mongolia, for his guidance throughout the process was invaluable to me.

This study has been supported by a CREST project (The Rangeland Atmosphere – Hydrosphere – Biosphere Interaction Study Experimental in Northeastern Asia) of JST (Japan Science and Technology Agency). I appreciate many supports from this project and the member of CREST for giving chance to study my own country.

Finally, I express special thanks to my family, friends and everyone else who gave me advice, much time, and support throughout the past years. Thank you a lot of!

References

Adyasuren, Ts., and Bayarjargal, Yu., (1992): Studies of vegetation change on the territory of Mongolia using AVHRR and meteorological ground data. Proceedings of the 13th Asian Conference on Remote Sensing, Ulaanbaatar, Mongolia, D-9.

Adyasuren, Ts., and Bayarjargal, Yu., (1995): Vegetation & drought monitoring using sattelite & ground data. International Workshop on Space Informatics for Sus. Develop.: Grassland Monitoring & Management. Ulaanbaatar, 20 June, Mongolia.

Adyasuren. Ts., Byambakhuu, I., Matsushima, D., Ganbaatar, T., Munkhbat, Ts., and Sugita, M., (2004): Some results of Spectral Reflectance of Some Associations in the Kherlen River basin under RAISE project, The 3nd International Workshop on Terrestrial Change in Mongolia, 9-10 November, Tsukuba, Ibaraki, Japan

Asner, G., (1998): Biophysical and biochemical sources of variability in canopy reflectance. Remote. Sens. Environ 64, 234-253

Asner, G., and Lobell, B., (2000): A biogeophysical approach for automated SWIR unmixing of soil and vegetation. Remote Sensing of Environment. 74, 99-112

Asner, G., and Heidebrecht, K.B., (2002): Spectral unmixing of vegetation, soil and dry carbon in arid regions: Comparing multi-spectral and hyperspectral observations Int. J. Remote Sens.

Batesom, C., Asner, G., and Wessman, C., (2000): Endmember bundles: a new approach to incorprorating endmember variability into spectral mixture analysis. IEEE Trans Geosci Remote Sen. 38(2): 1083-94

Bayarjargal, Yu., (1995): Estimation of grassland primary production and carrying capacity at the Hustain-Nuruu Nature Reserve. Project Final Report, IMH, Ulaanbaatar, pp.15.

Byambakhuu, I., Sugita. M., Matsushima, D., and Adyasuren. Ts., (2006): Assessment of regional land cover fractions of mongolian semiarid and arid area based on multi-

channel Radiance Data. , The 5nd International Workshop on Terrestrial Change in Mongolia, 28-29 November, Tokyo, Japan

Carlson, T., and Ripley, D., (1997): On the relationship between NDVI, fractional vegetation cover, and leaf area index. Remote Sensing of Environment 62, 241-252

Erdenetuya, M., (2004): Remote sensing methodology and technology for pasture vegetation monitoring of Mongolia. Dissertation of Ph.D thesis, NUM, Ulaanbaatar, Mongolia.

Kimes, D., (1983): Dynamic of directional reflectance factor distribution for vegetation canopies. Appl. Opt. 22, 1364-1372.

Li, X., Chen, Y., Yang, H., and Zhang Y., (2005): Improvement, comprason, and application of field measurement methods for grassland vegetation fractional Coverage. Journal of Integrative Plant Biology. 49 (9): 1074-1083

Oyun, R., Bayarjargal, Yu., and Enkhbayar, M., (1994): Development of methodology for estimation of grassland primary production at the Hustain NN.R.. Fin.report, Ulanbaatar, pp. 80.

Oyun, R., Batbayar, L., Tungalag, D., (2000): Climate change and its impacts in Mongolia, National Agency for Meteorology, Hydrology and Environment Monitoring, JEMR publishing.

Rahman, H., Verstraete, M., and Pinty, B., (1993): Coupled surface-atmoshpere reflectance (CSAR) model, 1. Model description and inversion on synthetic data, J. Geophys. Res., 98, 20779-20789.

Roujean, L., Leroy, M., and Deschamps, P., (1992): A bidirectional reflectance model of the Earth surface for the correction of remote sensing data. J.Geophys. Res 97, 20455-20468

Shiirevdamba, Ts., (1998): Biological Diversity in Mongolia, *First National Report, Ministry for Nature and the Environment,* 'Admon' printing house, Ulaanbaatar, Mongolia, pp. 106.

Susaki, J., Hara, K., Kajiwara, K., and Honda, Y., (2004): Robust estimation of BDRF model parameter, Remote Sens. Env. 89, 63-71.

White, M, Asner, G, Nemani, R, Rrivette, J, Running, S (2000): Measuring fractional cover and leaf area index in arid ecosystem: Digital camera, radiation transmittance, and laser altimetry methods. Remote Sens. Environ. 74, 45 -57

Zhou, Q., Robson, M., and Pilesjo., P (1998): On the ground eatimation of vegetation cover in Australasian rangelands. Int. J. Remote Sens. 19, 1815 -1820